Commission of the European Communities

nuclear science and technology

AN EXPLICIT "ALE" FINITE ELEMENT FORMULATION FOR 3D TRANSIENT DYNAMIC FLUID-STRUCTURE INTERACTION PROBLEMS

J. DONEA, S. GIULIANI
Commission of the European Communities
Joint Research Centre
I-21020 ISPRA (VARESE)

Directorate-General Science, Research and Development
Joint Research Centre

1989

EUR 11936 EN

Published by the
COMMISSION OF THE EUROPEAN COMMUNITIES

Directorate-General
Telecommunications, Information Industries and Innovation

L-2920
LUXEMBOURG

LEGAL NOTICE

Abstract

Finite element models, implemented in the computer code EURDYN-3M, are presented for the prediction of the non-linear response of three-dimensional fluid-structure systems exposed to transient dynamic loading.

An arbitrary Lagrangian-Eulerian kinematical description of the fluid domain is adopted in which the grid points can be displaced independently of the fluid motion. This formulation leads to an easy and accurate treatment of fluid-structure interfaces and permits significant fluid sloshing and swirling to occur without producing excessive distorsions of the computational mesh.

Two numerical examples are presented to illustrate the potential of the proposed modelling procedures.

Contents

1 Introduction

The analysis of problems in nuclear reactor safety and in several other engineering fields often requires a study of fluid-structure systems exposed to transient dynamic loading. For example, the evaluation of structural integrity of reactor components under postulated energy excursions involves the analysis of structures of complex shape and their interaction with the fluid in which they are embedded. Furthermore, during these energy excursions both the fluid and the structure undergo non-linear response.

These needs for safety evaluations have motivated the developement of computational methods capable to treat transient, non-linear fluid-structure interaction problems. Until fairly recently, numerical solutions to problems of fluid-structure interaction have been achieved by the finite difference method. Rather than attempting a necessarily superficial survey of the many computational techniques developed in this area (see for istance [1] for an overview), we simply wish here to underline the leader role played by the Los Alamos, Livermore, and Argonne groups in these developements.

In recent years, the alternative finite element method (FEM), well proven in the structural mechanics field, has been successfully extended to deal with problems in fluid mechanics. Such extension, combined to the natural ability of the FEM to arbitrarily mix fluid and structural subdomains, has originated a new and very versatile computational technique for problems of fluid-structure interaction.

Applications of FEM to hydro-structural problems have first been reported by Belytschko and Kennedy [2] and then by Donea, Giuliani and Fasoli-Stella [3]. In these studies, a purely Lagrangian method was employed for the kinematical description of the fluid domain. This approach is limited by its inability to cope easily with the strong distorsions which often characterize flows of interest.

Furthermore, although a clear delineation of fluid-structure interfaces is in principle afforded by the Lagrangian description, a complicated slide-surface logic has to be introduced to treat the relative sliding at the interface between an inviscid fluid and a structure. On the other hand, if the fluid motion were described in Eulerian coordinates, strong distorsions could be handled with relative ease, but at the expense of precise interface definition and great complexity in handling fluid-structure coupling.

Because of the shortcomings of purely Lagrangian and purely Eulerian descriptions, efforts have recently been expended in the finite element area to develop integrated procedures with generalized kinematical descriptions of the fluid domain that possess both Eulerian and Lagrangian features.

These generalized descriptions are usually referred to as mixed Lagrangian-Eulerian, or Arbitrary Lagrangian-Eulerian (ALE) methods and were originally developed by Noh, Trulio and Hirt, Amsden and Cook [4,5,6] in finite difference formats. The theoretical framework for mixed Lagrangian-Eulerian finite element descriptions has been established by Hughes et al. [7] in the context of viscous, incompressible flows. ALE finite element methods for inviscid, compressible flows have been reported by Belytschko et al. and Donea et al. [8,9,10,11,15,17,20].

The purpose of the present report is to describe an ALE finite element method with automatic and continuous rezoning of the fluid mesh developed at the Joint Research Centre Ispra to predict the response of three-dimensional fluid-structure systems subjected to transient dynamic loading.

We first recall the basic concepts underlying the Arbitrary Lagrangian-Eulerian description and present the ALE form of the basic equations governing the flow of a compressible, inviscid fluid.

This is followed by a description of the ALE fluid analysis algorithm which includes space discretization by finite elements, numerical time integration of the semi-discrete equations and a discussion of the prescription we propose for the automatic motion of the hydrodynamic grid.

The structural analysis algorithm is then presented and fluid-structure coupling in the ALE formulation discussed.

Finally, two numerical examples are presented to illustrate the potential of the proposed modelling procedures.

2 The Arbitrary Lagrangian-Eulerian formulation

In this section, we first recall the basic theoretical concepts underlying the Arbitrary Lagrangian-Eulerian (ALE) formulation.

To start with, a brief account is given of the classical concepts of Lagrangian and Eulerian descriptions of the motion of a continuum. Then the ALE description is introduced and the notion of material derivative in this generalized kinematical description is examined.

On this basis, we derive ALE differential forms for the basic conservation equations of mass, momentum and energy and develop the associated weak variational forms which provide a basis for the formulation of finite element models.

2.1 Lagrangian and Eulerian descriptions of motion

Consider a continuum B in the N-dimensional vector space R^N (N=1,2 or 3) with basis e_i, $i = 1,\ldots,N$ and an open time interval $\sqsupset 0,T \sqsubset \in R$. We shall use the terms *particle* or *material point* to denote a small volumetric element of the continuum B. The motion of B is described by the trajectories along which the material points of the continuum move in space.

Be X a material point of B. During time, B always consists of the same material points though its configuration vary. We shall denote by R_X the configuration of B at the initial time t_0 and by R_x its configuration at the present time t ; R_X is called the material domain and R_x the spatial domain.

In the initial configuration R_X , a representative particle of the continuum occupies a point P_0 in space (see Fig.1) and has the position vector

$$\mathbf{X} = (X_i),\ i = 1,\ldots,N \tag{1}$$

with respect to rectangular Cartesian axes. In the current configuration R_x, the particle originally at P_0 is located at the point P and has the position vector

$$\mathbf{x} = (x_i),\ i = 1,\ldots,N \tag{2}$$

The coordinates X_i are called *material coordinates*, while the coordinates x_i are called *spatial coordinates*.

The motion of B during time is described by the application

$$\Phi : R_X \times \sqsupset 0, T \sqsubset \rightarrow R^N, \tag{3}$$

$$\mathbf{X}, t \rightsquigarrow \mathbf{x} \tag{4}$$

such that, at any fixed time t, the image of R_X be R_x and the image of $\mathbf{X} \in R_X$ be $\mathbf{x} \in R_x$. This yields the system of equations

$$x_i = \Phi_i(X_j, t),\ i = 1, \ldots, N \tag{5}$$

which relates the components of the position vectors $\mathbf{X}$ and $\mathbf{x}$ of the material point X in the material domain R_X and in the spatial domain R_x. Equation (5) may be interpreted as a mapping of the initial configuration of the continuum into its current configuration.

It is assumed that such a mapping is one-to-one and continuous, with continuous partial derivatives to whatever order is required. As a consequence, the Jacobian of trasformation (5) should not vanish

$$J = \left| \frac{\partial x_i}{\partial X_j} \right| \neq 0 \tag{6}$$

In these conditions, there exists an inverse for transformation (5) which reads

$$X_i = \Psi_i(x_j, t),\ i = 1, \ldots, N \tag{7}$$

Equation (7) may be interpreted as one which provides a tracing to its original position of the particle that now occupies the location $\mathbf{x}$.

The displacement vector $\mathbf{u}$ from R_X to R_x is defined by

$$\mathbf{u} = \mathbf{x} - \mathbf{X} \tag{8}$$

The components of $\mathbf{u}$ can be expressed either in terms of the material coordinates of X through the law of motion (5) :

$$\mathbf{u} = u_i(X_j, t) e_i \tag{9}$$

or in terms of the spatial coordinates of X through (7) :

$$\mathbf{u} = U_i(x_k, t)e_i \tag{10}$$

The representation (9) of the displacement is called *Lagrangian*, while representation (10) is called *Eulerian*.

It is noted that the Lagrangian description of motion fixes the attention on the material points of the continuum, while the Eulerian description considers a fixed portion of the space occupied by the continuum and examines what goes on there during time. It follows that in the Lagrangian description the mesh of grid points moves with the continuum, while in the Eulerian description the computational mesh is kept fixed and the continuum moves through it.

2.2 ALE description of motion

The Arbitrary Lagrangian-Eulerian (ALE) description represents a generalization of the purely Lagrangian and purely Eulerian descriptions of the motion of a continuum. In fact, the ALE description fixes the attention neither on material points nor on a fixed region of space, but on what we shall call *reference points* which may be moving with the continuum, but independently from the motion of its material points.

In order to introduce the law of motion of the reference points, it is convenient to consider, in addition to the material and spatial domains R_X and R_x, a third domain R_ξ, called *referential domain*. This referential domain will play for the reference points the role played by R_X for the material points.

With reference to the same rectangular Cartesian axes as before, let

$$\xi = (\xi_i),\ i = 1, \ldots, N \tag{11}$$

represent the position vector of a reference point Q_0 in the initial configuration of the referential domain R_ξ (see fig.1). The coordinates ξ_i of the reference point Q_0 are called *mixed coordinates*.

One then defines the motion of the reference points by the application

$$\hat{\mathbf{\Phi}} : R_\xi \times \sqsupset 0, T \sqsubset \rightarrow R^N \tag{12}$$

$$\xi, t \rightsquigarrow \mathbf{x} \tag{13}$$

such that, at any fixed time t, the image of R_ξ be R_x and any given point $\mathbf{x}$ of the spatial domain R_x be the image of a reference point $\boldsymbol{\xi} \in R_\xi$. One therefore writes

$$x_i = \hat{\Phi}_i(\xi_j, t), i = 1, \ldots, N \tag{14}$$

and it is assumed that the vector function $\hat{\boldsymbol{\Phi}}$ and its partial derivatives to whatever order is required are continuous in ξ_j and t.

In addition, for the mapping represented by $\hat{\boldsymbol{\Phi}}$ to be one-to-one, the mixed Jacobian $\tilde{J}$ of transformation (14) should not vanish

$$\tilde{J} = \left| \frac{\partial x_i}{\partial \xi_j} \right| \neq 0 \tag{15}$$

At this point, it is important to note that, at any time t, one may associate with each point $\mathbf{x}$ of the spatial domain R_x one material point P with coordinates X_j in the material domain R_X and one reference point Q with coordinates ξ_j in the reference domain R_ξ

$$\mathbf{x} = \boldsymbol{\Phi}(X_j, t) = \hat{\boldsymbol{\Phi}}(\xi_j, t) \tag{16}$$

Clearly, the above two points only coincide in $\mathbf{x}$ at a given time t. Later on, each of these points will move with its own law of motion.

For the material points, the velocity $\mathbf{v}$ at time t is given by the time derivative of the position vector (5) taken with $\mathbf{X}$ held fixed

$$\mathbf{v} = \left. \frac{\partial \mathbf{x}(X_j, t)}{\partial t} \right|_{\mathbf{X}} = \left. \frac{\partial \mathbf{u}(X_j, t)}{\partial t} \right|_{\mathbf{X}} \tag{17}$$

Relation (17) gives a Lagrangian representation of the velocity.

As far as the reference points are concerned, the displacement vector $\hat{\mathbf{u}}$ from R_ξ to R_x is given by

$$\hat{\mathbf{u}} = \mathbf{x} - \boldsymbol{\xi} = \hat{\mathbf{u}}(\xi_k, t) \tag{18}$$

Therefore, the velocity $\mathbf{w}$ of the reference points is given by

$$\mathbf{w} = \left. \frac{\partial \mathbf{x}(\xi_k, t)}{\partial t} \right|_{\xi} = \left. \frac{\partial \hat{\mathbf{u}}(\xi_k, t)}{\partial t} \right|_{\xi} \tag{19}$$

By specializing the definition of the reference domain R_ξ and of the law $\hat{\mathbf{\Phi}}$ of its motion, one can recover the classical kinematical descriptions. For instance, selecting $R_\xi = R_X$ and $\hat{\mathbf{\Phi}} = \mathbf{\Phi}$ yields the Lagrangian description for which relations (18,19) give

$$\hat{\mathbf{u}} = \mathbf{x} - \mathbf{X} = \mathbf{u} \tag{20}$$

$$\mathbf{w} = \mathbf{v} \tag{21}$$

On the other hand, choosing $R_\xi = R_x$ and $\hat{\mathbf{\Phi}}$ as the identity transformation, we recover the Eulerian description. In this case, $\boldsymbol{\xi} = \mathbf{x}$ and relations (18,19) give

$$\hat{\mathbf{u}} = \mathbf{w} = \mathbf{0} \tag{22}$$

Summarizing, we have seen that the ALE description has no basic dependence on particles and treats the computational mesh as a reference frame which may be moving with an arbitrary velocity $\mathbf{w}$. Depending on the value of the velocity $\mathbf{w}$, the following basic viewpoints may be individuated:

1. $\mathbf{w} = 0$: the computational mesh is fixed in space; this corresponds to the Eulerian viewpoint.

2. $\mathbf{w} = \mathbf{v}$: the mesh moves in space at the same velocity as the particles; this corresponds to the Lagrangian viewpoint.

3. $\mathbf{w} \neq \mathbf{v} \neq \mathbf{0}$: the mesh moves in space at a velocity $\mathbf{w}$ which is in principle arbitrary; this is the ALE viewpoint. Details on the practical selection of the mesh velocity $\mathbf{w}$ are given in section 3.2.

2.3 Material, spatial and mixed derivatives

Let us consider a physical property F of the continuum B and denote by $f(x_j,t)$, $f^*(X_j,t)$ and $f^{**}(\xi_j,t)$ its spatial, material and mixed representations, respectively. In order to evaluate the time rate-of-change of property F, one has the choice between three types of derivative :

- The *material derivative* is the variation of F per unit time felt by an observer moving with the material points. It is here denoted by the symbol $\frac{DF}{Dt}$.

- The *spatial derivative* of F is the variation per unit time at a fixed point in space; it is here represented by the notation $\left.\frac{\partial F}{\partial t}\right|_{\mathbf{x}}$.
- The *mixed derivative* of F is the variation per unit time felt by an observer moving with the reference points; it is here represented by the notation $\left.\frac{\partial F}{\partial t}\right|_{\xi}$.

When F is in material representation, its material derivative is readily calculated, since

$$\frac{DF}{Dt} = \left.\frac{\partial f^*(X_j,t)}{\partial t}\right|_{\mathbf{X}} \tag{23}$$

When F is given in spatial representation, its material derivative includes two terms and is given by

$$\frac{DF}{Dt} = \left.\frac{\partial f}{\partial t}\right|_{\mathbf{x}} + \left.\frac{\partial f}{\partial x_j}\right|_t \left.\frac{\partial x_j}{\partial t}\right|_{\mathbf{X}} \tag{24}$$

$$= \left.\frac{\partial f}{\partial t}\right|_{\mathbf{x}} + v_j(x_k,t)\left.\frac{\partial f}{\partial x_j}\right|_t \tag{25}$$

The first term in the right-hand side of (25) is the spatial derivative and the second term is the convective term of the material derivative.

Finally, when F is given in mixed representation by $f^{**}(\xi_j,t)$, its material derivative reads

$$\frac{DF}{Dt} = \left.\frac{\partial f^{**}}{\partial t}\right|_{\xi} + \left.\frac{\partial f^{**}}{\partial \xi_j}\right|_t \left.\frac{\partial \xi_j}{\partial t}\right|_{\mathbf{X}} \tag{26}$$

The first term in the right-hand side of (26) is the mixed derivative of F; the second term is the convective term which may be expressed in terms of the relative velocity $(\mathbf{v}-\mathbf{w})$ of the material point with respect to the reference point. To see this, we consider relation (16), i.e.

$$x_j = \Phi_j(\mathbf{X},t) = \hat{\Phi}_j(\xi,t) \tag{27}$$

and take its partial derivative with respect to time with X held fixed. One obtains

$$\left.\frac{\partial x_j}{\partial t}\right|_{\mathbf{X}} = \left.\frac{\partial \Phi_j}{\partial t}\right|_{\mathbf{X}} = \left.\frac{\partial \hat{\Phi}_j}{\partial t}\right|_{\xi} + \left.\frac{\partial \hat{\Phi}_j}{\partial \xi_i}\right|_t \left.\frac{\partial \xi_i}{\partial t}\right|_{\mathbf{X}} \tag{28}$$

or, in view of the definitions (17) of the particle velocity **v** and (19) of the reference point velocity **w**:

$$v_j = w_j + \left.\frac{\partial x_j}{\partial \xi_i}\right|_t \left.\frac{\partial \xi_i}{\partial t}\right|_{\mathbf{X}} \tag{29}$$

Expression (29) indicates that

$$\left.\frac{\partial \xi_i}{\partial t}\right|_{\mathbf{X}} = (v_j - w_j) \left.\frac{\partial \xi_i}{\partial x_j}\right|_t \tag{30}$$

so that expression (26) of the material derivative in mixed description can be transformed into

$$\frac{DF}{Dt} = \left.\frac{\partial f^{**}}{\partial t}\right|_\xi + (v_j - w_j) \left.\frac{\partial f^{**}}{\partial \xi_i}\right|_t \left.\frac{\partial \xi_i}{\partial x_j}\right|_t \tag{31}$$

or, equivalently

$$\frac{DF}{Dt} = \left.\frac{\partial f^{**}}{\partial t}\right|_\xi + (v_j - w_j) \left.\frac{\partial f(\mathbf{x},t)}{\partial x_j}\right|_t \tag{32}$$

As we shall see in the next section, expression (32) of the material derivative in mixed description is of fundamental importance for the formulation of ALE differential forms of the basic conservation equations for mass, momentum and energy.

2.4 Conservation laws in the ALE description

To simplify the subsequent developements, we shall write the material derivative in the ALE description given in (32) in the form

$$\frac{D}{Dt} = F^* + c_i F_{,i} \tag{33}$$

where F^* indicates the partial derivative with respect to time for a given reference point ξ, while c_i represents the components of the relative velocity of the material point X with respect to the reference point ξ, i.e.

$$c_i = v_i - w_i \tag{34}$$

In (33) and the following equations, a comma followed by an index indicates partial derivative with respect to the corresponding spatial coordinate.

With the above notations, the equations which govern the continuum in the ALE description are the following three conservation equations (see references [13,15,20] for details):

- *Mass equation*

$$\varrho^* + c_i \varrho_{,i} = -\varrho v_{i,i} \tag{35}$$

- *Momentum equation*

$$\varrho v_i^* + \varrho c_j v_{i,j} = \sigma_{ji,j} + \varrho b_i, \;\; i = 1, \ldots, N \tag{36}$$

- *Energy equation*

$$\varrho e^* + \varrho c_i e_{,i} = \left(\sigma_{ij} v_i\right)_{,j} + \varrho b_i v_i \tag{37}$$

In relations (35-37), ϱ is the density, σ_{ij} Cauchy stress tensor, **b** body forces per unit mass and e the total internal energy given by

$$e = i + \frac{1}{2} v_i v_i \tag{38}$$

where i is the specific internal energy. Thermal effects have been neglected in the form (37) of energy conservation.

One may also write an *internal energy equation* in the form

$$\varrho i^* + \varrho c_i i_{,i} = \sigma_{ij} D_{ij} \tag{39}$$

where

$$D_{ij} = \frac{1}{2}(v_{i,j} + v_{j,i}) \tag{40}$$

is the rate of deformation (or stretching) tensor. Since

$$\varrho i^* = (\varrho i)^* - i \varrho^* \tag{41}$$

we note that, using the mass equation (35), the internal energy equation may be rewritten in the computationally more attractive form

$$(\varrho i)^* + c_i (\varrho i)^*_{,i} + \varrho i v_{i,i} = \sigma_{ij} D_{ij} \tag{42}$$

For an inviscid compressible fluid one has

$$\sigma_{ij} = -p\delta_{ij} \tag{43}$$

where p is the pressure and δ_{ij} the Kronecher delta. In this case

$$\sigma_{ij}D_{ij} = -pv_{i,i} \tag{44}$$

and the internal energy equation (42) reads

$$(\varrho i)^{*} + c_i(\varrho i)_{,i} = -(\varrho i + p)v_{i,i} \tag{45}$$

2.5 Weak variational form of the ALE conservation equations

We shall now develop weak variational forms of the ALE conservation laws which will provide the basis for space discretization using finite element modelling.

2.5.1 Mass equation

The ALE differential form (35) of the mass equation may be rewritten as

$$\frac{\partial \varrho}{\partial t} = (\mathbf{w} - \mathbf{v}) \cdot \nabla \varrho - \varrho \nabla \cdot \mathbf{v} \tag{46}$$

where, for simplicity, the time derivative ϱ^{*} for an observer moving with the reference points is noted $\frac{\partial \varrho}{\partial t}$.

Multiplying this equation by an arbitrary weighting function Ψ and integrating over a control volume $V(t)$, we obtain the following weak form of the mass conservation equation,

$$\int_{V(t)} \Psi \frac{\partial \varrho}{\partial t}\, dV = \int_{V(t)} \Psi(\mathbf{w} - \mathbf{v}) \cdot \nabla \varrho\, dV - \int_{V(t)} \Psi \varrho \nabla \cdot \mathbf{v}\, dV \tag{47}$$

A useful particular form of (47) may be derived by assuming that the density is constant over the control volume $V(t)$. In this case, we have $\nabla \varrho = 0$ and the weighting function Ψ may be chosen as unity. It follows that (47) reduces to the simple form

$$\int_{V(t)} \frac{\partial \varrho}{\partial t}\, dV = -\int_{V(t)} \varrho \nabla \cdot \mathbf{v}\, dV = -\oint_{S(t)} \varrho \mathbf{v} \cdot \mathbf{n}\, dS \tag{48}$$

which may be further transformed into

$$\frac{d}{dt}\int_{V(t)} \varrho\, dV = \oint_{S(t)} \varrho(\mathbf{w}-\mathbf{v})\cdot\mathbf{n}\, dS \tag{49}$$

This integral form of the statement of conservation of mass will be employed in finite element models assuming an elementwise uniform density. In passing from (48) to (49) we have used the identity

$$\frac{dV}{dt} = \nabla\cdot\mathbf{w}\, dV \tag{50}$$

2.5.2 Internal energy equation

The weak form of the internal energy equation (45) is derived in complete analogy with what has been done for the mass equation. It reads

$$\int_{V(t)} \Psi\frac{\partial}{\partial t}(\varrho i)\, dV = \int_{V(t)} \Psi(\mathbf{w}-\mathbf{v})\cdot\nabla(\varrho i)\, dV - \int_{V(t)} \Psi(\varrho i+p)\,\nabla\cdot\mathbf{v}\, dV \tag{51}$$

If the density of internal energy ϱi is assumed uniform over the control volume $V(t)$, the following integral statement may be deduced from the weak form (51) of the internal energy equation

$$\frac{d}{dt}\int_{V(t)} \varrho i\, dV = \oint_{S(t)} \varrho i(\mathbf{w}-\mathbf{v})\cdot\mathbf{n}\, dS - \int_{V(t)} p\,\nabla\cdot\mathbf{v}\, dV \tag{52}$$

This integral form will be used in connection with ALE finite element models in which an elementwise uniform density of internal energy is assumed.

2.5.3 Momentum equations

For an inviscid fluid, the ALE differential form (36) of momentum conservation reduces to the simple form

$$\varrho\frac{\partial v_i}{\partial t} = \varrho(\mathbf{w}-\mathbf{v})\cdot\nabla v_i + \varrho b_i - \frac{\partial p}{\partial x_i} \tag{53}$$

Equation (53) must be supplemented with appropriate boundary conditions. We shall assume that on portion S_1 of the boundary the velocity

is prescribed, whereas on the remaining portion S_2 the components T_i of boundary loads are imposed

$$-n_j\delta_{ji}p = T_i \tag{54}$$

The weak form of the momentum equation is obtained multiplying (53) by an arbitrary admissible (i.e. vanishing on S_1) variation δv_i of the fluid velocity followed by integration over $V(t)$. After integration by parts of the pressure term, use of the divergence theorem and of the stress boundary relation (54), the following result is obtained

$$\begin{aligned}\int_{V(t)} \delta v_i \varrho \frac{\partial v_i}{\partial t}\, dV \;=\; & \int_{V(t)} \delta v_i \varrho (\mathbf{w}-\mathbf{v})\cdot\nabla v_i\, dV + \\ & \int_{V(t)} \delta v_i \varrho b_i\, dV + \\ & \int_{V(t)} p\frac{\partial}{\partial x_i}(\delta v_i)\, dV + \\ & \oint_{S_2(t)} \delta v_i T_i\, dS\end{aligned} \tag{55}$$

Equation (55) provides the basis for the formulation of spatially discrete models of the momentum equations using finite element approximations.

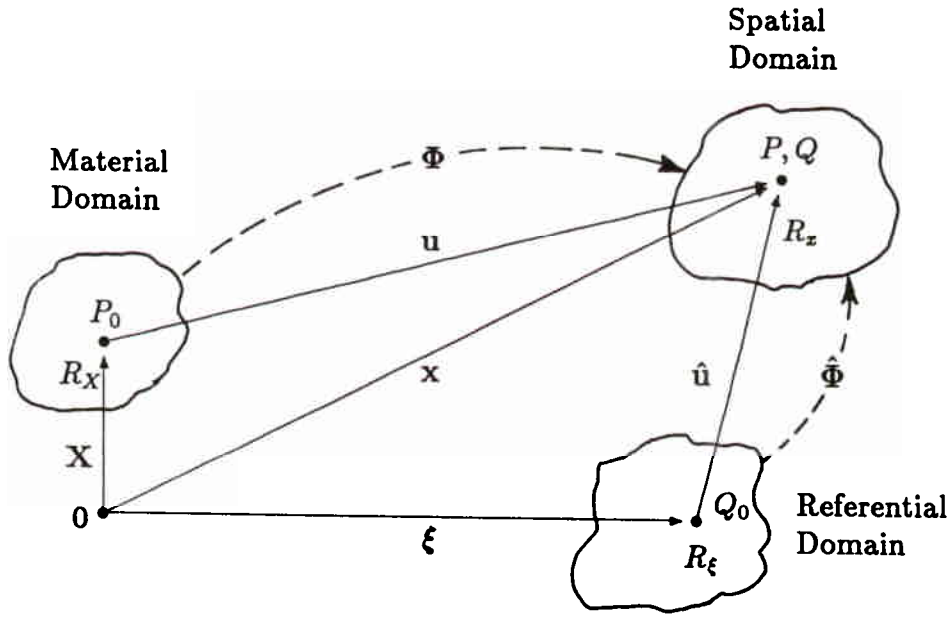

Figure 1: Schematic diagram of domains and mappings for the ALE description.

3 Fluid analysis algorithm

Three distinct tasks are involved in the construction of an ALE finite element algorithm for transient fluid flow. These are :

1. to derive spatially discrete models of the ALE conservation equations using finite element modelling;
2. to prescribe the kinematics of the hydrodynamic mesh, i.e., to specify the nodal values of the grid velocity $\mathbf{w}$;
3. to integrate the semi-discrete conservation equations forward in time to obtain the transient response.

3.1 Spatially discrete models

For the purpose of providing a framework for our discussion of spatially discrete models of the ALE conservation equations, we will first define the basic variables in the form of local approximations over a typical finite element. We will use the following notation :

- u_i lower case subscripts denote components of a vector;
- u_I upper case subscripts denote node numbers;
- e denotes a typical finite element;
- $\cdot$ denotes a time derivative.

The usual assumption in discretizing partial differential equations in finite element schemes is that the functional dependence of the variables in space and time can be separated, so that any local vector field $u_i(x,t)$ in an element can be described as product of shape functions $N_I(x)$ that are independent of time and nodal values $u_{iI}(t)$ which are independent of x and incorporate the time dependence

$$u_i(\mathbf{x},t) = N_I(\mathbf{x})u_{iI}(t) \tag{56}$$

Here the fluid velocity $\mathbf{v}$ and the arbitrary grid velocity $\mathbf{w}$ will be interpolated over a typical finite element by the same shape functions

$$\begin{aligned} v_i(\mathbf{x},t) &= N_I(\mathbf{x})v_{iI}(t) \\ w_i(\mathbf{x},t) &= N_I(\mathbf{x})w_{iI}(t) \end{aligned} \tag{57}$$

Another set of shape functions is usually employed for the local description of the density ϱ and for the density of internal energy ϱi

$$\begin{aligned} \varrho(\mathbf{x},t) &= \Phi_J(\mathbf{x})\varrho_J(t) \\ \varrho i(\mathbf{x},t) &= \Phi_J(\mathbf{x})\varrho i_J(t) \end{aligned} \tag{58}$$

While shape functions N must ensure inter-element continuity of the velocities $\mathbf{v}$ and $\mathbf{w}$, this is not necessarily the case for shape functions Φ. In general, the fluid properties in (58) are interpolated by a polynomial which is at least one order less than that for the velocities.

In the remainder of this report, the discussion of 3D fluid finite element models will be restricted to the 8-node hexahedral element which has been implemented in the computer code EURDYN-3M. For the fluid domain discretization, 4, 5 and 6-node elements (tetrahedron, pyramid and prism) are also employed but they are treated by the code as hexahedral elements in which some nodes are coincident. The density and specific internal energy are assumed elementwise constant and a trilinear local approximation is used to describe the fluid and mesh velocities.

3.1.1 Semi-discrete mass equation

In updating the mass of an element, the integral form (49) of the conservation of mass is used, which gives

$$\frac{dM^e}{dt} = \frac{d}{dt}\int_{V^e} \varrho\, dV = \sum_J \varrho_J \int_{S_J} (\mathbf{w}-\mathbf{v})\cdot\mathbf{n}\, dS \tag{59}$$

where $\sum_J$ indicates a summation over the eight faces S_J of element e, and the velocities are evaluated in terms of nodal values as indicated by (57).

To stabilize the mass equation, the density ϱ_J is computed as a weighted average of the densities in the elements e and e' on either side of face J

$$\varrho_J = \frac{1}{2}[(1-\alpha_J)\varrho^e + (1+\alpha_J)\varrho^{e'}] \tag{60}$$

For the evaluation of the coefficient α_J we first compute the flux F through face J by

$$F = \int_{S_J} (\mathbf{w} - \mathbf{v}) \cdot \mathbf{n}\, dS \tag{61}$$

If F is positive, the flux is entering the element e and density $\varrho^{e'}$ is favoured in the weighted average in equation (60) by choosing $\alpha_J > 0$. Conversely, if F is negative the flux leaves element e and density ϱ^e is favoured by choosing $\alpha_J < 0$. To satisfy these requirements we take

$$\alpha_J = \alpha_0\, Sign(F) \tag{62}$$

where $0 \leq \alpha_0 \leq 1$; $\alpha_0 = 1$ gives a full donor approximation, $\alpha_0 = 0$ corresponds to a centered approximation.

3.1.2 Semi-discrete internal energy equation

Proceeding as described in the previous section for the mass equation and noting that the pressure, defined by an equation of state of the form $p = f(\varrho, i)$, is constant over the element, from (52) we can derive the rate of change of internal energy in an element by

$$\frac{d}{dt}\int_{V^e} \varrho i\, dV = \sum_J (\varrho i)_J \int_{S_J} (\mathbf{w} - \mathbf{v}) \cdot \mathbf{n}\, dS - p^e \oint_{S^e} \mathbf{v} \cdot \mathbf{n}\, dS \tag{63}$$

The energy density ϱi is computed by

$$(\varrho i)_J = \frac{1}{2}[(1 - \alpha_J)(\varrho i)^e + (1 + \alpha_J)(\varrho i)^{e'}] \tag{64}$$

where α_J is function of α_0 as in (62) and the flux F is given by (61)

3.1.3 Semi-discrete momentum equations

The principle of virtual power (55) is applied to derive the semi-discrete equations expressing conservation of momentum in the finite element mesh. According to the Galerkin method, the velocity variation is defined as

$$\delta v_i = N_I(\mathbf{x})\delta v_{iI} \tag{65}$$

where the N_I's are the velocity shape functions defined in (57). Independent variations of all velocity degrees of freedom in the mesh are introduced in turn into the principle of virtual power (55) and by invoking the arbitrariness of such variations, the discrete analog to the momentum equations is obtained.

The semi-discrete equation governing a typical node I is found in the form

$$\begin{aligned}\sum_e \int_{V^e} N_I \varrho N_J \dot{v}_{iJ}\, dV &= \sum_e \int_{V^e} N_I \varrho (w_j - v_j) \frac{\partial N_J}{\partial x_j} v_{iJ}\, dV + \\ &\quad \sum_e \int_{V^e} N_I (\varrho b_i - \frac{\partial p}{\partial x_i})\, dV - \\ &\quad \sum_e \oint_{S^e_{ext}} N_I T_i\, dS \end{aligned} \tag{66}$$

where $\sum_e$ indicates a summation over all the elements to which the node I belongs, the repetition of subscript J implies a summation over all nodes in element e, and subscript i denotes components of a vector. The governing equations for the discrete mesh form a set of ordinary differential equations in time which may be written in condensed form as

$$[M]\dot{\mathbf{v}} = \mathbf{F}_t + \mathbf{F}_b + \mathbf{F}_p + \bar{\mathbf{F}} \tag{67}$$

where

- $[M]$ is the global mass matrix consisting, as shown in (66), of element contributions of the type

$$M^e_{IJ} = \int_{V^e} \varrho N_I N_J\, dV \tag{68}$$

- $\dot{\mathbf{v}}$ denotes the global vector of nodal accelerations;

- $\mathbf{F}_t$ indicates global nodal loads induced by transport of momentum; as shown by (66), a typical component of vector $\mathbf{F}_t$ is obtained by assembly of element contributions of the form

$$(F_{t_{iI}})^e = \int_{V^e} N_I \varrho (w_j - v_j) \frac{\partial N_J}{\partial x_j} v_{iJ}\, dV \tag{69}$$

- $\mathbf{F}_b$ denotes global nodal loads due to body forces ϱb_i

$$(F_{b_{iI}})^e = \int_{V^e} N_I \varrho b_i \, dV \tag{70}$$

- $\mathbf{F}_p$ represents the nodal loads induced by the fluid pressure p

$$(F_{p_{iI}})^e = \int_{V^e} p \frac{\partial N_I}{\partial x_i} \, dV \tag{71}$$

- $\bar{\mathbf{F}}$ accounts for the externally applied loads T_i

$$(\bar{\mathbf{F}}_{iI})^e = \int_{S^e_{ext}} N_I T_i \, dS \tag{72}$$

An artificial viscous pressure, q, is added to the fluid pressure p when calculating shock propagation problems. The viscous pressure used in EURDYN-3M is composed, as suggested by Wilkins [23], of a quadratic and a linear term in the divergence of the fluid velocity:

$$q = \begin{cases} \varrho[C_A^2 l^2 (\nabla \cdot \mathbf{v})^2 - C_L l \, a \nabla \cdot \mathbf{v}] & \text{when} \quad \nabla \cdot \mathbf{v} < 0 \\ 0 & \text{when} \quad \nabla \cdot \mathbf{v} \geq 0 \end{cases} \tag{73}$$

In this expression, $l = \sqrt[3]{V_e}$, where V_e is the element volume, a is the dilatational wave speed and C_A, C_L are numerical coefficients. According to Wilkins et al. [23], $C_A \approx 2$, $C_L \approx 0.8$ for explicit Lagrangian calculations.

Anti-hourglassing forces may also be applied in EURDYN-3M to control zero energy modes which arise due to one-point integration of first-order isoparametric elements. The formulation suggested by Flanagan and Belytschko [24] has been implemented.

3.2 Automatic mesh displacement prescription algorithm

The freedom in moving the fluid mesh offered by the ALE formulation is very attractive. However, it can be overshadowed by the burden of specifying grid velocities $\mathbf{w}$ well suited to a particular problem. As a consequence, the practical implementation of the ALE description requires that an automatic mesh displacement prescription algorithm be supplied.

In the following paragraph we describe an automatic mesh displacement prescription algorithm for three-dimensional finite element meshes consisting of 8, 6, 5 and 4-node elements (hexahedron, prism, pyramid and tetrahedron). These elements with linear, or trilinear local velocity field are the only 3D hydrodynamic elements currently implemented in the J.R.C. Ispra ALE computer code EURDYN-3M. An early version of the 3D rezone algorithm was presented in [16].

3.2.1 Rezoning of a generic node.

Consider, as shown in fig.2, a portion of a three-dimensional finite element mesh consisting of hexahedral, prism, pyramid and/or tetrahedral elements. To a generic nodal point I we associate an influence domain (dashed in fig.2) defined by the set of tetrahedra obtained by joining node I to all nodes connected to it via the element sides.

The basic task of the rezone algorithm is to displace node I so as to render the tetrahedra defining its influence domain as regular as possible. In other words, we wish to minimize both the squeeze and the distorsion of each tetrahedron in the influence domain of a given node.

Let Δx_i, $i = 1,2,3$ be the displacements of node I required to achieve its rezone (i indicates x, y, z components). Consider a generic tetrahedron (I, J, K, L) in the influence domain of node I as shown in fig.2; after rezone the tetrahedron basis area a (opposite to node I) and height h are given respectively by

$$a = \sqrt{pp + qq + rr} \tag{74}$$

$$h = (p\Delta x_1 + q\Delta x_2 + r\Delta x_3 + 3v')/a \tag{75}$$

where, v' indicates the volume of the tetrahedron before rezoning

$$v' = (px_{1I} + qx_{2I} + rx_{3I} + u)/3 \tag{76}$$

while p, q, r, u are the following determinants

$$p = \frac{1}{2}\begin{vmatrix} x_{2J} & x_{3J} & 1 \\ x_{2K} & x_{3K} & 1 \\ x_{2L} & x_{3L} & 1 \end{vmatrix}$$

$$
\begin{aligned}
q &= -\frac{1}{2}\begin{vmatrix} x_{1J} & x_{3J} & 1 \\ x_{1K} & x_{3K} & 1 \\ x_{1L} & x_{3L} & 1 \end{vmatrix} \\
r &= \frac{1}{2}\begin{vmatrix} x_{1J} & x_{2J} & 1 \\ x_{1K} & x_{2K} & 1 \\ x_{1L} & x_{2L} & 1 \end{vmatrix} \\
u &= -\frac{1}{2}\begin{vmatrix} x_{1J} & x_{2J} & x_{3J} \\ x_{1K} & x_{2K} & x_{3K} \\ x_{1L} & x_{2L} & x_{3L} \end{vmatrix}
\end{aligned} \tag{77}
$$

The total volume V of the influence domain and its mean height $\bar{h}$ are

$$
\begin{aligned}
V &= \sum_n v' \\
\bar{h} &= \frac{3V}{\sum_n a}
\end{aligned} \tag{78}
$$

where n represents the number of tetrahedra in the influence domain. The coordinates of the centroid of the triangle defined by nodes J, K, L (fig.3) are

$$
\bar{x}_i = (x_{iJ} + x_{iK} + x_{iL})/3, \; i = 1, 2, 3 \tag{79}
$$

and the distances between J, K, L and the centroid are

$$
\begin{aligned}
D_J &= \sqrt{\sum_{i=1}^{3}(x_{iJ} - \bar{x}_i)^2} \\
D_K &= \sqrt{\sum_{i=1}^{3}(x_{iK} - \bar{x}_i)^2} \\
D_L &= \sqrt{\sum_{i=1}^{3}(x_{iL} - \bar{x}_i)^2}
\end{aligned} \tag{80}
$$

The projection of I on the lines joining the centroid and J, K, L gives the points J', K', L' (fig.3) and the distances between these points and the centroid are

$$
D'_J = \sum_{i=1}^{3}(x_{iI} + \Delta x_i - \bar{x}_i) * (x_{iJ} - \bar{x}_i)/D_J
$$

$$
\begin{aligned}
D'_K &= \sum_{i=1}^{3}(x_{iI} + \Delta x_i - \bar{x}_i) * (x_{iK} - \bar{x}_i)/D_K \\
D'_L &= \sum_{i=1}^{3}(x_{iI} + \Delta x_i - \bar{x}_i) * (x_{iL} - \bar{x}_i)/D_L
\end{aligned} \tag{81}
$$

These distances are clearly a measure of the distorsion of the tetrahedron, while the difference $h - \bar{h}$ is a measure of its squeeze. Considering the influence domain of node I as a whole we define

$$
E = W_1 \sum_n (h - \bar{h})^2 + W_2 \sum_n [(D'_J)^2 + (D'_K)^2 + (D'_L)^2] = minimum \tag{82}
$$

as a criterion for minimizing globally the squeeze and distorsion of the tetrahedra in the influence domain, where

$$
\begin{aligned}
W_1 &= \frac{1}{\bar{h}} \\
W_2 &= \frac{n}{4\sum_n (D_J^2 + D_K^2 + D_L^2)}
\end{aligned} \tag{83}
$$

The minimization of (82) with respect to Δx_i yields a system of linear equations

$$
[S]\{\Delta x_i\} = \{R\} \tag{84}
$$

where the elements of the symmetric matrix $[S]$ and of the right-hand vector $\{R\}$ are

$$
\begin{aligned}
S_{11} &= W_1 \sum_n \frac{p^2}{a^2} + \\
&\quad W_2 \sum_n \left[\frac{(x_{1J} - \bar{x}_1)^2}{D_J^2} + \frac{(x_{1K} - \bar{x}_1)^2}{D_K^2} + \frac{(x_{1L} - \bar{x}_1)^2}{D_L^2} \right] \\
S_{12} &= W_1 \sum_n \frac{pq}{a^2} + \\
&\quad W_2 \sum_n \left[\frac{(x_{1J} - \bar{x}_1)(x_{2J} - \bar{x}_2)}{D_J^2} + \frac{(x_{1K} - \bar{x}_1)(x_{2K} - \bar{x}_2)}{D_K^2} + \right. \\
&\quad \left. \frac{(x_{1L} - \bar{x}_1)(x_{2L} - \bar{x}_2)}{D_L^2} \right] \\
S_{13} &= W_1 \sum_n \frac{pr}{a^2} +
\end{aligned}
$$

$$W_2 \sum_n \left[\frac{(x_{1J} - \bar{x}_1)(x_{3J} - \bar{x}_3)}{D_J^2} + \frac{(x_{1K} - \bar{x}_1)(x_{3K} - \bar{x}_3)}{D_K^2} + \frac{(x_{1L} - \bar{x}_1)(x_{3L} - \bar{x}_3)}{D_L^2} \right]$$

$$S_{22} = W_1 \sum_n \frac{q^2}{a^2} + W_2 \sum_n \left[\frac{(x_{2J} - \bar{x}_2)^2}{D_J^2} + \frac{(x_{2K} - \bar{x}_2)^2}{D_K^2} + \frac{(x_{2L} - \bar{x}_2)^2}{D_L^2} \right]$$

$$S_{23} = W_1 \sum_n \frac{qr}{a^2} + W_2 \sum_n \left[\frac{(x_{2J} - \bar{x}_2)(x_{3J} - \bar{x}_3)}{D_J^2} + \frac{(x_{2K} - \bar{x}_2)(x_{3K} - \bar{x}_3)}{D_K^2} + \frac{(x_{2L} - \bar{x}_2)(x_{3L} - \bar{x}_3)}{D_L^2} \right]$$

$$S_{33} = W_1 \sum_n \frac{r^2}{a^2} + W_2 \sum_n \left[\frac{(x_{3J} - \bar{x}_3)^2}{D_J^2} + \frac{(x_{3K} - \bar{x}_3)^2}{D_K^2} + \frac{(x_{3L} - \bar{x}_3)^2}{D_L^2} \right]$$

$$R_1 = -W_1 \sum_n \frac{p}{a} \left(\frac{3V'}{a} - \bar{h} \right) - W_2 \sum_n [(x_{1J} - \bar{x}_1)P_J + (x_{1K} - \bar{x}_1)P_K + (x_{1L} - \bar{x}_1)P_L]$$

$$R_2 = -W_1 \sum_n \frac{q}{a} \left(\frac{3V'}{a} - \bar{h} \right) - W_2 \sum_n [(x_{2J} - \bar{x}_2)P_J + (x_{2K} - \bar{x}_2)P_K + (x_{2L} - \bar{x}_2)P_L]$$

$$R_3 = -W_1 \sum_n \frac{r}{a} \left(\frac{3V'}{a} - \bar{h} \right) - W_2 \sum_n [(x_{3J} - \bar{x}_3)P_J + (x_{3K} - \bar{x}_3)P_K + (x_{3L} - \bar{x}_3)P_L]$$

If T_0 denotes the determinant of the matrix $[S]$ the solution of the linear

algebraic system (84) is

$$\begin{aligned}
\Delta x_1 &= \frac{1}{T_0}\begin{vmatrix} R_1 & S_{12} & S_{13} \\ R_2 & S_{22} & S_{23} \\ R_3 & S_{32} & S_{33} \end{vmatrix} \\
\Delta x_2 &= \frac{1}{T_0}\begin{vmatrix} S_{11} & R_1 & S_{13} \\ S_{21} & R_2 & S_{23} \\ S_{31} & R_3 & S_{33} \end{vmatrix} \\
\Delta x_3 &= \frac{1}{T_0}\begin{vmatrix} S_{11} & S_{12} & R_1 \\ S_{21} & S_{22} & R_2 \\ S_{31} & S_{32} & R_3 \end{vmatrix}
\end{aligned} \tag{85}$$

3.2.2 Rezoning of a node with displacement constraints

If the nodal displacement is constrained to lie in a plane, the minimization of E in (82) with this constraint gives

$$\Delta x_i = \sum_{j=1}^{2} C_{ji} t_j, \; i = 1,2,3 \tag{86}$$

where C_{1i} and C_{2i}, $i = 1,2,3$ are the direction cosines of two orthogonal directions lieing in the plane and t_1, t_2 are easily obtained by solving the following system of equations

$$\begin{bmatrix} \sum_{i=1}^{3} C_{1i}\left(\sum_{j=1}^{3} C_{1j}S_{ij}\right) & \sum_{i=1}^{3} C_{1i}\left(\sum_{j=1}^{3} C_{2j}S_{ij}\right) \\ \sum_{i=1}^{3} C_{2i}\left(\sum_{j=1}^{3} C_{1j}S_{ij}\right) & \sum_{i=1}^{3} C_{2i}\left(\sum_{j=1}^{3} C_{2j}S_{ij}\right) \end{bmatrix} \begin{Bmatrix} t_1 \\ t_2 \end{Bmatrix} = \begin{Bmatrix} \sum_{i=1}^{3} C_{1i}R_i \\ \sum_{i=1}^{3} C_{2i}R_i \end{Bmatrix} \tag{87}$$

If the nodal displacement is constrained to occur along a line with direction cosines $C_i, i = 1,2,3$, the minimization of E in (82) with this constraint gives

$$\Delta x_i = C_i t^*, \; i = 1,2,3 \tag{88}$$

where t^* is given by

$$t^* = \frac{\sum_{i=1}^{3} C_i R_i}{\sum_{i=1}^{3} C_i (\sum_{j=1}^{3} C_j S_{ij})} \tag{89}$$

3.2.3 Implementation of the algorithm

The rezone algorithm described above has been implemented into the ALE finite element code EURDYN-3M. The code uses an explicit time-integration method and at each time station a first approximation to the grid velocity is computed for each ALE node by

$$\tilde{w}_i = w_i^{t-\Delta t} + \frac{\Delta x_i}{\Delta t} \tag{90}$$

where Δt is the time-step size and Δx_i are given by relations (85). Let f be for a given node the ratio of the grid velocity and the orthogonal projection on it of the fluid velocity. The components of the grid velocity computed by relation (90) are then limited by an empirical inequality of the type

$$(-\lambda) \leq f \leq (1+\lambda) \tag{91}$$

which is dictated by numerical stability and accuracy requirements. In expression (91) λ is a numerical coefficient ($0 \leq \lambda \leq 1$). The magnitude of the final grid velocity is then evaluated by

$$\begin{array}{ll} w_i^t = -\lambda v_i^t & \text{for : } f < -\lambda \\ w_i^t = \tilde{w}_i & \text{for : } -\lambda \leq f \leq (1+\lambda) \\ w_i^t = (1+\lambda) v_i^t & \text{for : } f > (1+\lambda) \end{array} \tag{92}$$

3.3 Numerical time integration

The algorithm for numerical time integration of the semi-discrete conservation equations for mass, momentum and internal energy is divided into two phases : Phase 1 is an explicit Lagrangian phase in which convective contributions are ignored and Phase 2, which is also explicit, is the convective phase.

Explicit time integration methods are only conditionally stable and the time-step size Δt must be limited so that sound waves do not travel more than one element during the time increment.

To enhance the numerical efficiency of explicit time integration algorithms, partitioning techniques are being used, in which different time steps are used in different parts of the mesh, so as to fully exploit local stability conditions. However, to simplify the exposition of the two phases in the

present time integration procedure, time integration based on a single time step will be considered first. Details on the practical implementation of partitioning techniques will be given in section 3.3.3.

The two phases in the explicit time integration are as follows :

3.3.1 PHASE 1 : Lagrangian calculation

Let superscript n denote the time level, so that $t^n = \sum_n \Delta t$ and $t^{n+1} = t^n + \Delta t$.

The fluid velocity at time $t^{n+1/2}$ is calculated first from the momentum equations (67) and using a diagonal mass matrix

$$\mathbf{v}^{n+1/2} = \mathbf{v}^{n-1/2} + \frac{\Delta t}{\mathbf{M}^n}[\mathbf{F}_t^* + \mathbf{F}_b^n + \mathbf{F}_p^n + \bar{\mathbf{F}}^n] \tag{93}$$

Here, $\mathbf{F}_t^*$ is the nodal load (69) induced by momentum transport arising from the previous time-step Phase 2 calculation (see eq.105 below).

Then, the following Lagrangian quantities (denoted by the superscript L) are evaluated :

- Nodal coordinates :

$$\mathbf{x}^L = \mathbf{x}^n + \Delta t\, \mathbf{v}^{n+1/2} \tag{94}$$

- Element volume :

$$V_e^L = f(\mathbf{x}^L) \tag{95}$$

- Element density :

$$\varrho_e^L = \frac{M_e^n}{V_e^L} \tag{96}$$

- Element internal energy and pressure (by iteration on 97 and 98) :

$$\begin{aligned} i_e^L &= i_e^n - p_e^n \frac{V_e^L - V_e^n}{M_e^n} \\ p_e^L &= f(\varrho_e^L, i_e^L) && (97) \\ i_e^L &= i_e^n - \frac{1}{2}\frac{(p_e^L + p_e^n)(V_e^L - V_e^n)}{M_e^n} && (98) \end{aligned}$$

The above L-values represent the end-of-step values in case of a purely Lagrangian calculation. In the Eulerian or ALE case, contributions from the convective terms in the conservation equations must be added to the time-advanced L-values. This is the objective of Phase 2.

3.3.2 PHASE 2 : Convective transport

We assume that the mesh velocities $\mathbf{w}^{n+1/2}$ have been evaluated using the automatic rezone atgorithm described in sections 3.2.1, 3.2.2 and 3.2.3. The following end-of-step quantities are then evaluated in sequence :

- Nodal coordinates :

$$\mathbf{x}^{n+1} = \mathbf{x}^n + \Delta t\, \mathbf{w}^{n+1/2} \tag{99}$$

- Element volume :

$$V_e^{n+1} = f(\mathbf{x}^{n+1}) \tag{100}$$

- Element mass (see eq.59) :

$$M_e^{n+1} = M_e^n + \Delta t \oint_{S_e^n} \varrho^L (w_j - v_j)^{n+1/2} n_j \, dS \tag{101}$$

- Element density :

$$\varrho_e^{n+1} = \frac{M_e^{n+1}}{V_e^{n+1}} \tag{102}$$

- Element internal energy (see eq.63) :

$$i_e^{n+1} = \frac{M_e^n}{M_e^{n+1}} i_e^L + \frac{\Delta t}{M_e^{n+1}} \oint_{S_e^n} \varrho_e^L i_e^L (w_j - v_j)^{n+1/2} n_j \, dS \tag{103}$$

- Element pressure :

$$p_e^{n+1} = f(\varrho_e^{n+1}, i_e^{n+1}) \tag{104}$$

- Nodal loads due to momentum transport (see eq.69) :

$$F_{tIi}^* = \int N_I \varrho_e^L (w_j - v_j)^{n+1/2} \frac{\partial v_i}{\partial x_j} \, dV \tag{105}$$

This completes the two steps contained in a cycle of the explicit time integration procedure.

3.3.3 Time partitioning

An explicit-explicit time partitioning, first introduced by Belytschko [21] (see also [22]), has been implemented in the code EURDYN-3M. It uses the following rules:

- fort each nodal point I, the critical time step Δt_I^c is the minimum critical time step found in the elements to which the node belongs;
- the time step Δt_I used in the integration of the equation of motion at each node is given by:

$$2^k \Delta t^c_{min} < \Delta t_I \leq 2^{k+1} \Delta t^c_{min} \tag{106}$$

  where Δt^c_{min} is the minimum critical time step found in the mesh and k is a positive integer;
- the element variables (density, internal energy and pressure) are updated whenever a new acceleration has to be computed at a

  node of the element. Linear displacement interpolations are used for the element nodes with larger critical time steps;
- when the node with the largest critical time step in the mesh has been integrated forward in time, all the element variables are advanced and a new time-partitioning cycle is entered.

With this technique the nodes with the smallest critical time step are integrated at every time step, while the other nodes are only periodically processed. The element computations required to evaluate the nodal loads are consequently reduced with respect to a procedure based on a single time step throughout the mesh.

This improves the efficiency of the numerical time integration process and saves computer time.

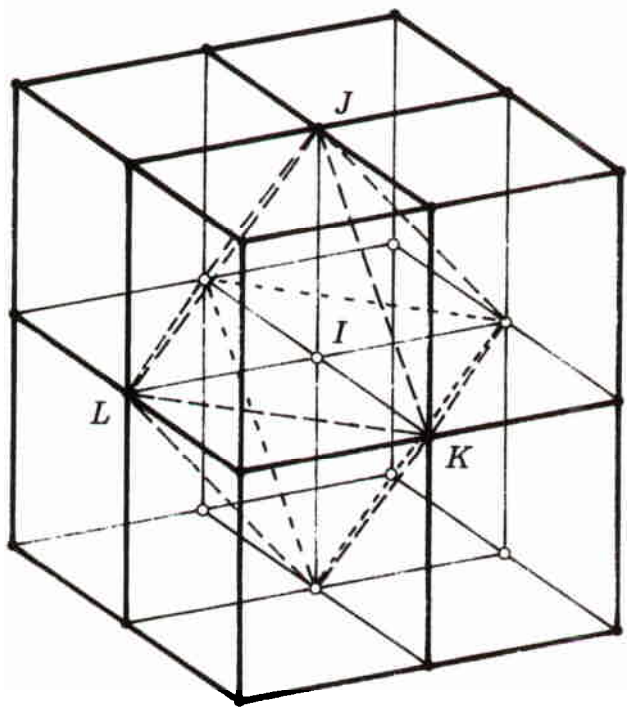

Figure 2: Influence domain of a node I in a three-dimensional mesh.

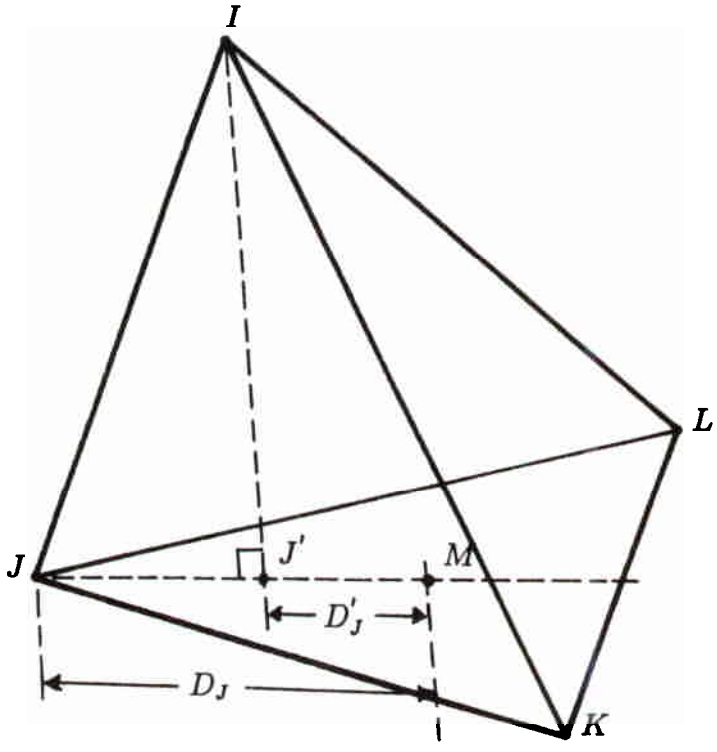

Figure 3: Generic tetrahedron in the influence domain of node I.

4 Structural analysis algorithm

A 4-node thin-shell element is used in EURDYN-3M to model the containment vessel in fluid-structure systems.

The element results from the degeneration of an 8-node isoparametric continuum element obtained upon introduction of classical thin-shell hypotheses. The formulation of the element follows the lines indicated by Hughes [25],[26],[27],[28] and is presented in detail by Casadei in reference [29].

The elastic-plastic response of the structural material is idealized through a trilinear stress-strain diagram. The material is assumed to satisfy the von Mises yield criterion and an isotropic hardening rule is considered. Numerical integration of the constitutive law is based on the classical elastic predictor-radial return concept.

An explicit central-difference method is used to update displacements and velocities in the structural mesh:

$$\mathbf{u}^{n+1} = \mathbf{u}^{n} + \Delta t\, \mathbf{v}^{n+1/2} \tag{107}$$

$$\mathbf{v}^{n+1/2} = \mathbf{v}^{n-1/2} + \Delta t\, \mathbf{a}^{n} \tag{108}$$

5 Fluid-structure coupling

Suitable conditions must be prescribed along fluid-solid interfaces to allow relative sliding of the fluid and solid. Two distinct techniques are employed in EURDYN-3M to deal with fluid-solid interfaces. The first applies to the permanently submerged parts of the structural domain and makes use of the freedom allowed by the ALE technique to force the fluid nodes to remain contiguous to the structural nodes, so that all nodes on the sliding interfaces remain permanently aligned. The second technique is used where fluid and solid nodes cannot be kept aligned, in this case Lagrangian sliding surfaces are employed.

5.1 ALE sliding surfaces

The purpose of this paragraph is to show that fluid-structure coupling may be achieved in a very simple and elegant manner if the fluid is treated in the ALE formulation.

5.1.1 Computation of nodal accelerations

In order to illustrate the coupling procedure along fluid-solid interfaces, let us consider a structural member embedded in a fluid which is allowed to slide along the faces of the structure. As shown in fig.4, two nodes are placed at each point of the interface: one fluid node and one structural node.

Since the fluid is treated in the ALE formulation, the movement of the fluid mesh may be chosen completely independent from the movement of the fluid itself. In particular, we may constrain the fluid nodes to remain contiguous to the structural nodes, so that all nodes on the sliding interface remain permanently aligned.

It is clear that such a permanent alignment of nodes along the interface greatly facilitates the flow of information between fluid and structural domains and permits fluid-structure coupling to be effected in the simplest manner.

The following conditions are prescribed at each point of the interface between an inviscid fluid and a deforming structure:

1. the grid velocity of the fluid coincides with the material velocity of the solid;
2. the normal velocity of the fluid coincides with the normal velocity of the solid;
3. the tangential velocities of the fluid and the solid are unconstrained.

In order to specify the above conditions, a local coordinate system t_1, t_2, n is set up at each node of the interface (fig.4), so that t_1 and t_2 lie in a plane tangent to the sliding interface and n is normal to it. See next paragraph for the selection of the tangent plane orientation.

Indicating by $\mathbf{w}$ the grid velocity and by $\mathbf{v}$ the material velocity and using the subscripts F, S to indicate the fluid and the solid and n, t_1, t_2 to indicate respectively the normal and tangential directions, referring to fig.4, the condition under point (1) implies that

$$\mathbf{w}_F = \mathbf{v}_S \tag{109}$$

The conditions under points (2) and (3) are enforced through the nodal loads. The condition of common normal velocity implies that

$$v_{Fn} = v_{Sn} \tag{110}$$

Since the two nodes must have a common normal velocity at all times, we prescribe that

$$\frac{d}{dt}[(\mathbf{v}_F - \mathbf{v}_S) \cdot \mathbf{n}] = 0 \tag{111}$$

or

$$(\dot{\mathbf{v}}_F - \dot{\mathbf{v}}_S) \cdot \mathbf{n} + (\mathbf{v}_F - \mathbf{v}_S) \cdot \frac{d\mathbf{n}}{dt} = 0 \tag{112}$$

Now

$$\frac{d\mathbf{n}}{dt} = \frac{\mathbf{n}^{t+\Delta t} - \mathbf{n}^t}{\Delta t} \tag{113}$$

and since

$$(\mathbf{v}_F - \mathbf{v}_S) \cdot \mathbf{n} = 0 \tag{114}$$

relation (112) reduces to

$$\dot{v}_{Fn} - \dot{v}_{Sn} = \frac{v_{Sn} - v_{Fn}}{\Delta t} \tag{115}$$

Thus, the condition of common normal velocity implies different normal accelerations at the two nodes if the normal to the interface changes direction with time. To evaluate these normal accelerations, we pose

$$\begin{aligned} \dot{v}_{Fn} &= a_n + a_{Fn} \\ \dot{v}_{Sn} &= a_n + a_{Sn} \end{aligned} \tag{116}$$

where a_n is a common normal acceleration, and a_{Fn}, a_{Sn} are individual complementary accelerations.

The common normal acceleration a_n is obtained from the equation of motion

$$(M_F + M_S)a_n = F_n \tag{117}$$

where, referring to fig.4, M_F and M_S are respectively the mass contributed by the elements adjacent to the fluid and solid nodes. The normal load F_n is obtained by transformation into the (t_1, t_2, n)-system of the assembled internal nodal loads F_i, $i = 1, 2, 3$ contributed by the relevant fluid and solid elements.

In view of (115 and 116), the complementary accelerations are linked by

$$a_{Fn} - a_{Sn} = \frac{v_{Sn} - v_{Fn}}{\Delta t} = A_n \tag{118}$$

and a second relationship between these accelerations may be obtained from the requirement of equilibrium which reads

$$M_F a_{Fn} + M_S a_{Sn} = 0 \tag{119}$$

It follows that

$$\begin{aligned} a_{Fn} &= \frac{M_S}{M_F + M_S} A_n \\ a_{Sn} &= \frac{-M_F}{M_F + M_S} A_n \end{aligned} \tag{120}$$

This completes the computation of normal accelerations which ensure a common normal velocity at the fluid and solid nodes on the interface.

The tangential velocities at the fluid and solid nodes are unconstrained and result from the equations of motion

$$M_S \dot{v}_{St_1} = F_{St_1}$$

$$
\begin{aligned}
M_S \dot{v}_{St_2} &= F_{St_2} \\
M_F \dot{v}_{Ft_1} &= F_{Ft_1} \\
M_F \dot{v}_{Ft_2} &= F_{Ft_2}
\end{aligned} \tag{121}
$$

where the tangential loads are again obtained by transformation into the (t_1, t_2, n)- system of the assembled internal forces F_i, $i = 1, 2, 3$.

5.1.2 Tangent plane orientation

In general the element faces around a node belonging to a sliding surface are not parallel. It follows that, if the tangent plane orientation is not properly defined, the fluid tangential velocity at the inteface node may produce a spurious transport of fluid across the intersecting sides.

The amount of fluid lost on some faces may be compensated by the amount gained on other faces by a suitable choice of the tangent plane orientation to which the tangential velocity is assumed to be parallel.

If S_i, $i = 1, 2, 3$ are the projections of the surfaces of the faces surrounding a given node on the planes $x_2 - x_3$, $x_3 - x_1$ and $x_1 - x_2$, an exact compensation of the spurious fluxes can be obtained by imposing the following condition

$$\sum_{i=1}^{3} v_i S_i = 0 \tag{122}$$

where v_i, $i = 1, 2, 3$ are the components of the tangential velocity in the global reference system x_1, x_2, x_3.

Posing

$$S = \sqrt{\sum_{i=1}^{3} S_i^2} \tag{123}$$

and dividing equation (122) by S we obtain

$$\sum_{i=1}^{3} \frac{v_i S_i}{S} = 0 \tag{124}$$

This means that the spurious transport of fluid vanishes if one selects the tangent plane as being perpendicular to the direction defined by the following direction cosines

$$\cos \alpha_i = \frac{S_i}{S}, \; i = 1, 2, 3 \tag{125}$$

5.2 Lagrangian sliding surfaces

Under some circumstances (e.g. near a fluid free surface), interface nodes cannot be kept aligned and Lagrangian sliding surfaces must be introduced to treat fluid-structure interaction.

The interface involves two Lagrangian surfaces: the first consists of fluid nodes while the second consists of structural nodes.

In EURDYN-3M the problem of fluid-structure coupling along Lagrangian sliding surfaces is faced by preparing a new fluid virtual surface, equivalent to the real one, but with nodes which coincide with those of the solid surface. It then follows that the nodes of the fluid virtual surface and of the solid surface are aligned and their accelerations can be computed as described in section 5.1.

5.2.1 Nodal masses and loads for fluid virtual surface

In the actual fluid sliding surface we define the domain D_I of a given node I as the sum of the surfaces of the element faces to which the node belongs. We assume that the loads F_i^{fc} and mass M^{fc} per unit surface in an element face are given by the sum over the nodes defining the face itself of the nodal loads and masses divided by their domain surface

$$\begin{aligned} F_i^{fc} &= \sum_I \frac{F_{iI}}{D_I} \\ M^{fc} &= \sum_I \frac{M_I}{D_I} \end{aligned} \tag{126}$$

where i indicates the vector components, and I the face nodes. Every face of the actual fluid surface covers one or several parts of the virtual surface faces (fig.5). The nodal loads and masses F_{iJ}, M_J of this last surface may be obtained from the contributions of every covered part S^p by the following integrals

$$\begin{aligned} F_{iJ} &= \int_{S^p} N_J F_i^{fc}\, dS \\ M_J &= \int_{S^p} N_J M^{fc}\, dS \end{aligned} \tag{127}$$

where F_i^{fc}, M^{fc} are the loads and mass per unit surface of the relevant face, and N_J are the corresponding shape functions. These integrals are numerically evaluated in the code using a 2×2 Gaussian rule.

5.2.2 Computation of nodal accelerations

Considering the fluid virtual surface and the solid surface and assuming the tangent plane orientation as defined in section 5.1.2 to obtain the (t_1, t_2, n)-system, the nodal normal accelerations can easily be computed by relation (117) while the tangential accelerations for the solid result from the equations of motion

$$\begin{aligned} M_S \dot{v}_{St_1} &= F_{St_1} \\ M_S \dot{v}_{St_2} &= F_{St_2} \end{aligned} \tag{128}$$

The normal acceleration for the actual fluid nodes is set equal to the normal acceleration at the adjacent point on the solid surface and computed using relation

$$\dot{v}_{Fn} = \sum_J N_J \dot{v}_{SnJ} \tag{129}$$

where N_J are the shape functions of the adjacent solid node and J the relevant nodes of the solid element face.

The tangential fluid accelerations, that are unconstrained, may be obtained from the equations of motion

$$\begin{aligned} M_F \dot{v}_{Ft_1} &= F_{Ft_1} \\ M_F \dot{v}_{Ft_2} &= F_{Ft_2} \end{aligned} \tag{130}$$

The complementary accelerations are computed using (120) where masses and velocities for the fluid are the nodal values while for the solid they are evaluated at the adjacent point in the solid face by the relations

$$\begin{aligned} v_{Sn} &= \sum_J N_J v_{SnJ} \\ M_S &= \sum_J N_J M_{SJ} \end{aligned} \tag{131}$$

For the fluid nodes the complementary accelerations are then added to those abtained by (129), while for the solid nodes they are multiplied by the shape functions and added to those obtained by (117).

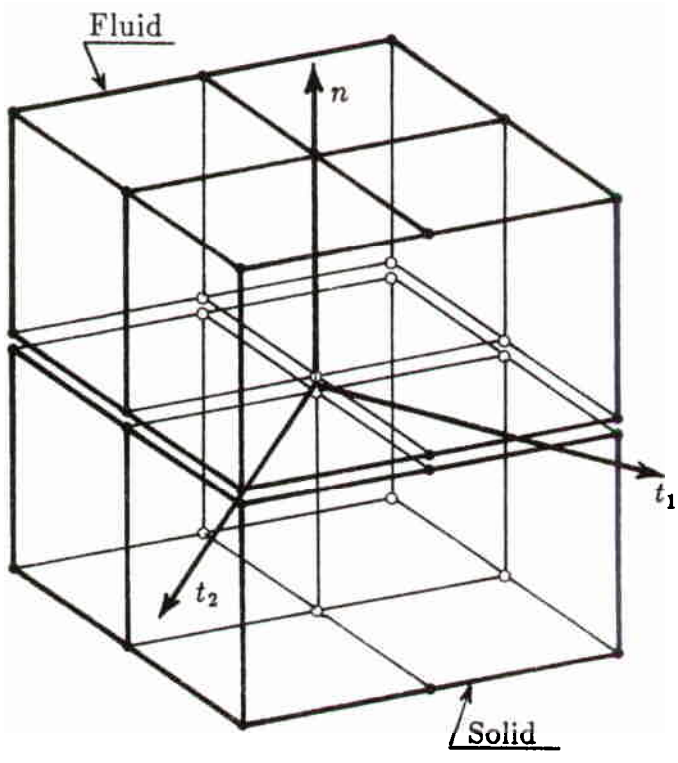

Figure 4: ALE sliding surfaces. Local coordinate system (t_1, t_2, n) at each node of the fluid-solid inteface.

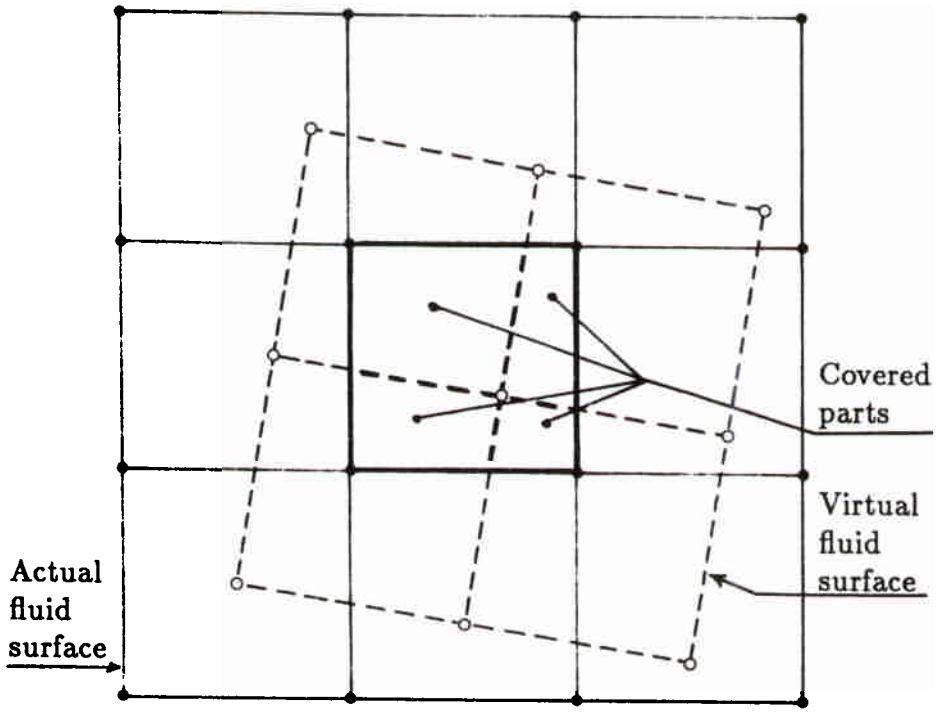

Figure 5: Lagrangian sliding surfaces. Actual and virtual fluid surface in the fluid-solid interface.

6 Applications

As an illustration of the ALE finite element modelling procedures discussed in the present paper, we shall present results for two test problems obtained using the new three-dimensional finite element computer code EURDYN-3M, release 1, recently developed at J.R.C. Ispra.

These two problems, the first of which is purely structural while the second involves fluid-structure interaction, have been chosen for their ability to validate the new code against existing reference solutions.

6.1 Spherical cap

An academic problem consisting of a rigidly clamped spherical cap (fig.6), externally loaded with a constant pressure $P(t) = 600$ starting at time $t = 0$, has been run to check the structural module of the EURDYN-3M code.

Only a symmetric sector has been discretized using 20 shell elements (fig.7) and suitable displacement and rotation constraints have been imposed to the nodes belonging to the symmetry plane.

The properties of the employed elastic-plastic material are (nondimensional units):

- initial density: 2.45×10^{-4};
- Poisson's ratio: 0.3;
- Young's modulus: 1.050×10^{7};
- bilinear stress-strain law (isotropic hardening):

  first yield stress: 2.4×10^{4};
  first hardening slope: 2.1×10^{5}.

Computed deformed meshes at various times are shown in fig.8. Histories of the external pressure work and of the apex deflection are shown in fig.9. Our computations are in good agreement with results obtained using different elements and codes [18].

6.2 Thin cylindrical vessel with hemispherical bottom

As example of fluid-structure interaction, the dynamic response of a thin cylindrical vessel with hemispherical bottom has been computed (fig.10). The vessel is nearly completely filled with water and loaded by the detonation of an explosive charge located on the axis. The top of the vessel is clamped on a rigid cover.

The employed finite element mesh for a symmetric sector of the configuration is shown in fig.12; it consists of 23 shell elements for the vessel and 258 hydrodynamic elements to model the charge and the water. The air gap above the water free surface is modelled as a void. Fig.11 shows the vessel thickness as a function of the distance from the rigid cover.

The interface between the explosive charge and the water, as well as the water free surface have been taken as purely Lagrangian. The rest of the hydrodynamic domain has been treated in the ALE formulation and the corresponding nodes have been moved automatically by the computer program.

Sliding of water along the flexible vessel has been treated in ALE form, except for the 9 edges near the free surface where Lagrangian sliding surfaces have been introduced to deal with interface nodes which do not remain aligned.

The properties of the explosive charge are [19]:

- initial density $\varrho_0 = 270\ (Kg/m^3)$;
- constitutive law:

$$\begin{aligned} P &= A[1 - E_2/(CV)]\exp^{-CV} \\ &\quad + B[1 - E_2/(DV)]\exp^{-DV} \\ &\quad + (\varrho_0 i - E_1)E_2/V \quad (MPa) \end{aligned}$$

where:

$V = \varrho_0/\varrho$;
$A = 17039.0$;
$B = 1159.5$;

$C = 9.0;$
$D = 2.4;$
$E_1 = 1029.0;$
$E_2 = 0.1;$

and: $\varrho_0 i_0 = 1629.0\ (MPa\, m^3/m^3)$.

The properties of the water are:

- initial density: $\varrho_0 = 1000\ (Kg/m^3)$;
- constitutive law:

$$P = 1.0 \times 10^5 P_1 P_2 + 2.0 B_3 \varrho i / V\ (MPa); \tag{132}$$

where:

$V = \varrho_0/\varrho;$
$P_1 = P_3(B_1 + A_1 P_3 - B_2 P_3^2)$
$P_2 = 1.0 - B_3(1 - V)/V$
if$(V = 1)$ then $P_3 = 0.0$
else $P_3 = \left[Z + \sqrt{Z^2 + A_2(1-V)^2}\right] / [A_3(1-V)]$
$Z = A_1(1 - V) - 1;$
$A_1 = 2.086;$
$A_2 = 0.8293;$
$A_3 = 2.796$
$B_1 = 0.1483;$
$B_2 = 1.398;$
$B_3 = 0.14$

and: $\varrho_0 i_0 = 0.0\ (MPa\, m^3/m^3)$.

The properties of the elstoplastic vessel material are:

- initial density: $7900\ (Kg/m^3)$;
- Poisson's ratio: 0.3333;

- Young's modulus: 1.93×10^5 (MPa);
- trilinear stress-strain law (isotropic hardening):

  first yield stress: 275.0 (MPa);
  first hardening slope: 5895.0 (MPa);
  second yield stress: 354.0 (MPa);
  second hardening slope: 1867.0 (MPa).

Fig.13 shows the deformed configurations of the computational mesh at times 1, 2, 3 and 4 ms. The important increase of the charge volume, the progressive impact of water on the rigid vessel-cover and the successive deformation of the vessel itself are clearly seen on the figures.

One also notes that the automatic mesh displacement prescription algorithm has performed quite well.

Fig.14 gives a comparison between the EURDYN-3M and EURDYN-1M (2D-axisymmetric) results for the meridional profiles of the longitudinal and hoop strains. A fairly good agreement between the two computations may be noted in spite of the coarse 3-D discretization employed in the circumferential direction.

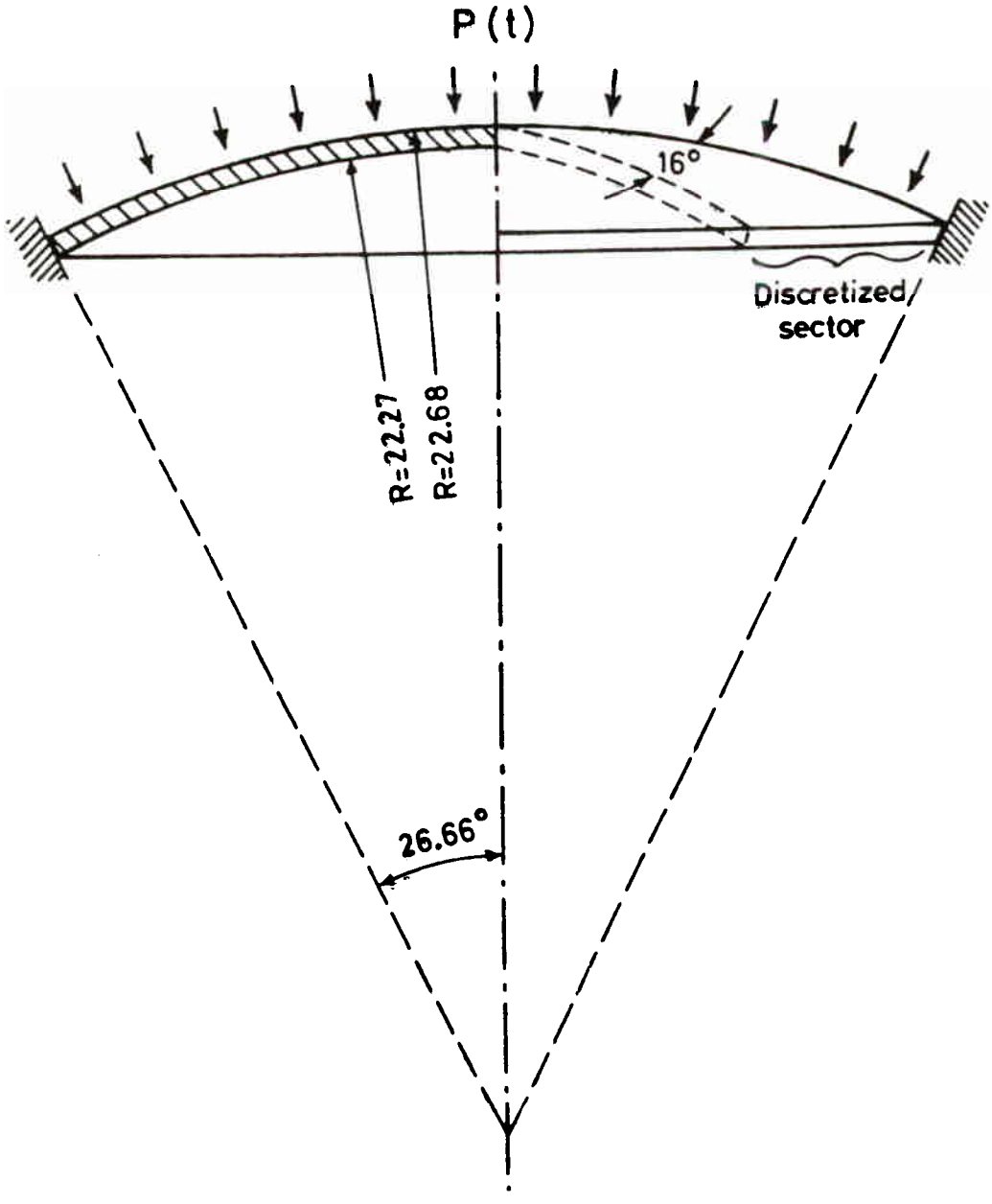

Figure 6: Spherical cap problem.

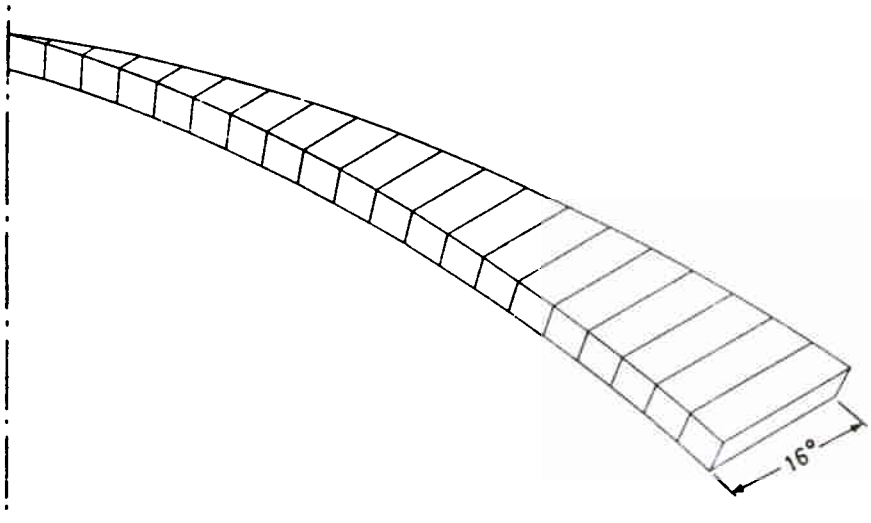

Figure 7: Finite element mesh for spherical cap problem.

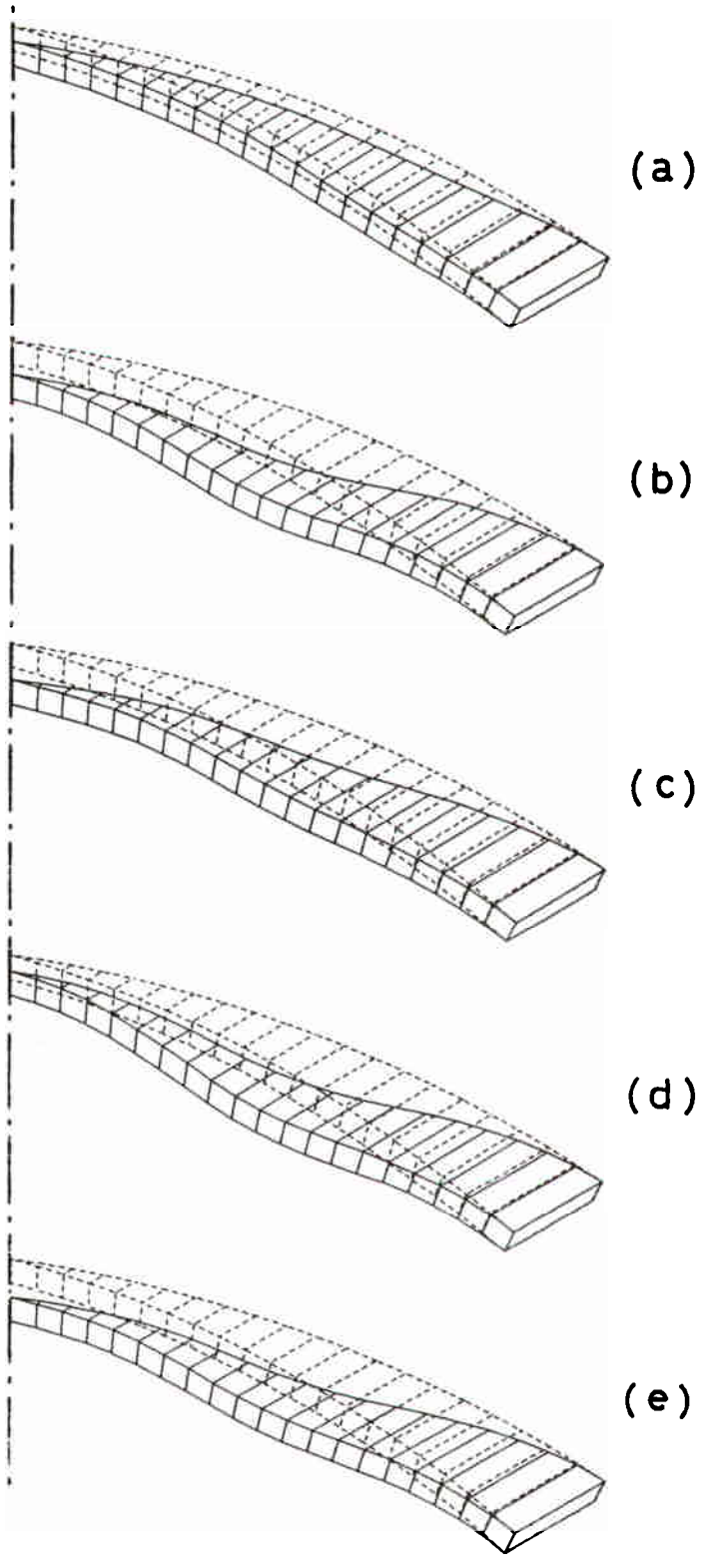

Figure 8: Spherical cap computation. Deformed mesh at various times (displacements magnification factor =10): (a) $t=1\times10^{-4}$; (b) $t=3\times10^{-4}$; (c) $t=5\times10^{-4}$; (d) $t=7\times10^{-4}$; (e) $t=8\times10^{-4}$.

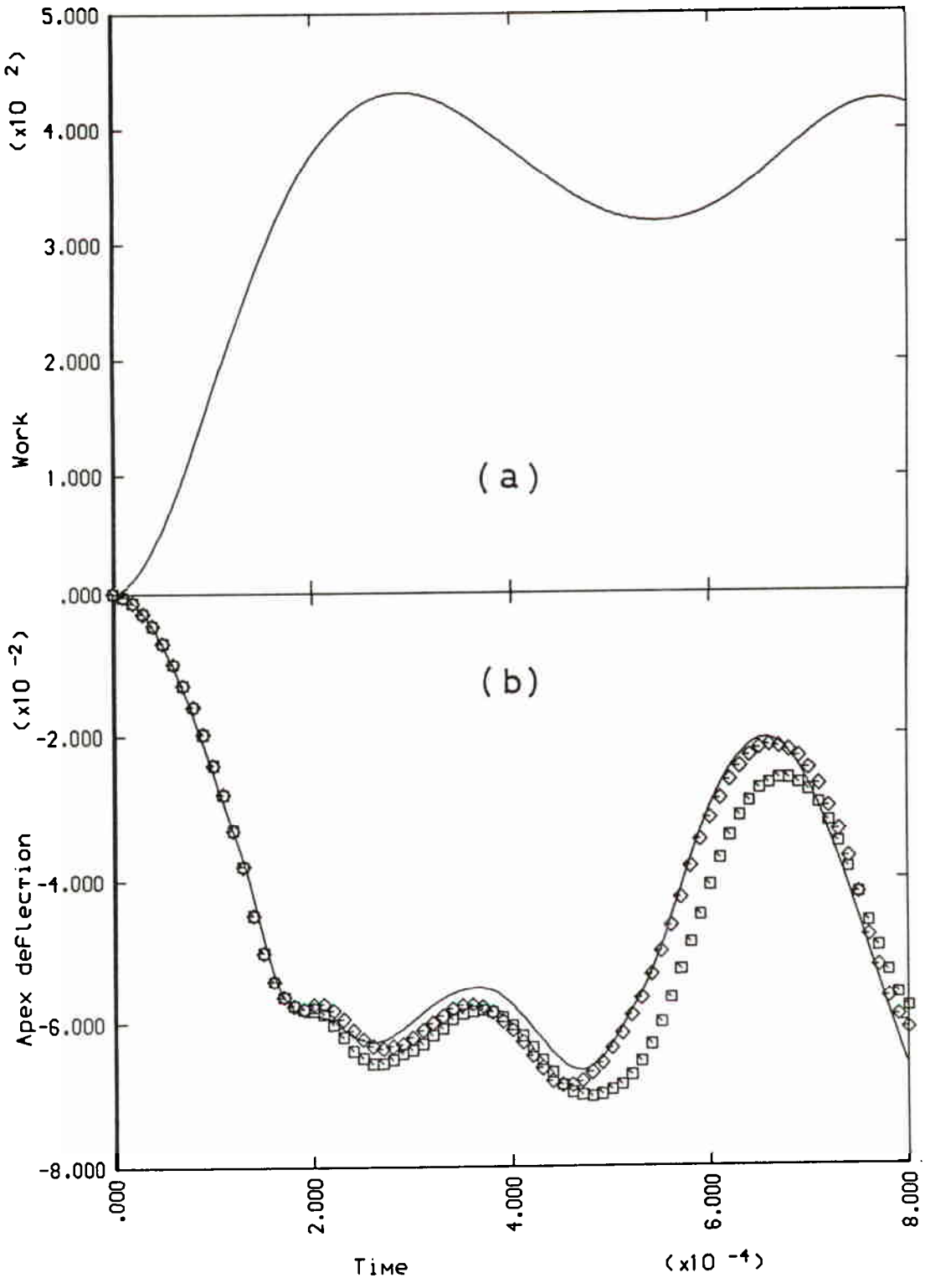

Figure 9: Spherical cap computation. Work done by external pressure (a) and apex deflection (b) versus time. —EURDYN-3M: 20 shell elements; ◇ EURDYN-2: 20 9-node elements; ⊡ EURDYN-1: 20 conical shell elements.

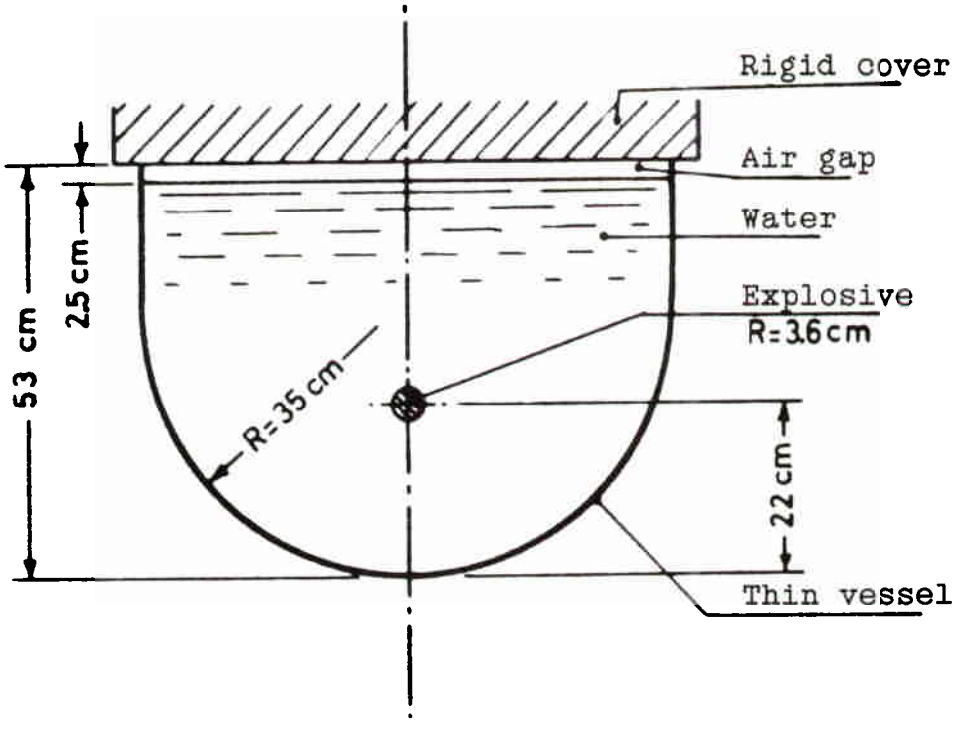

Figure 10: Thin cylindrical vessel problem.

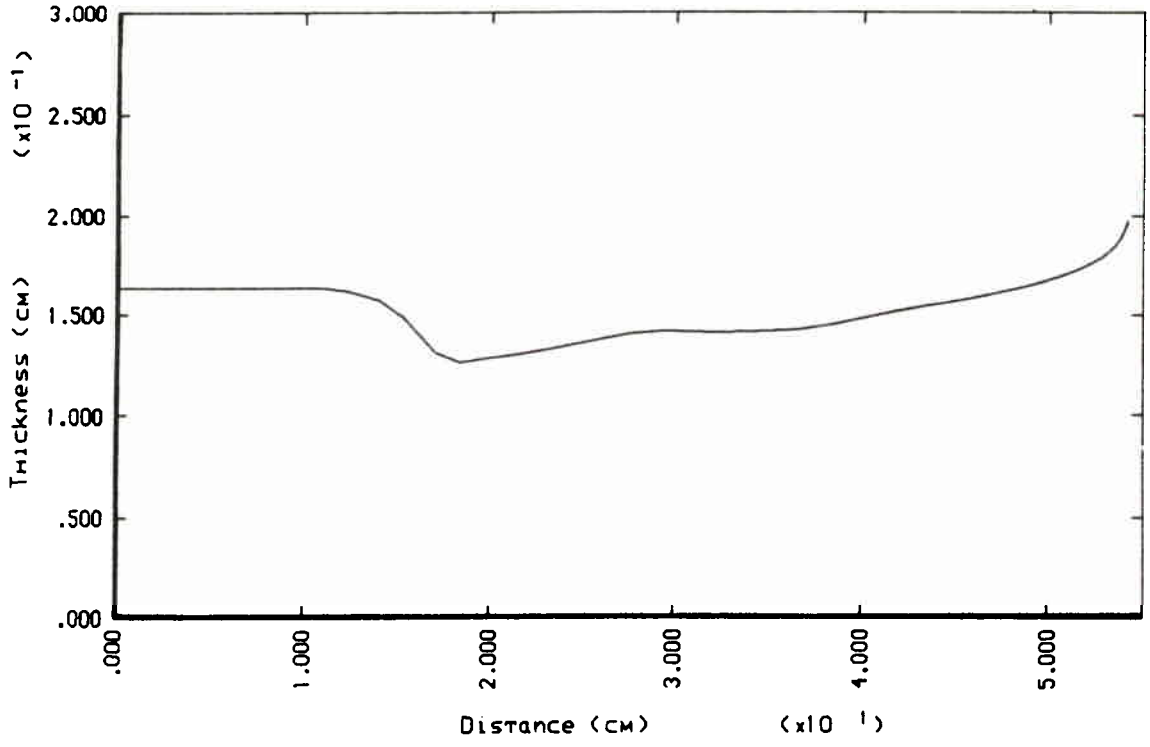

Figure 11: Vessel thickness versus distance from rigid cover.

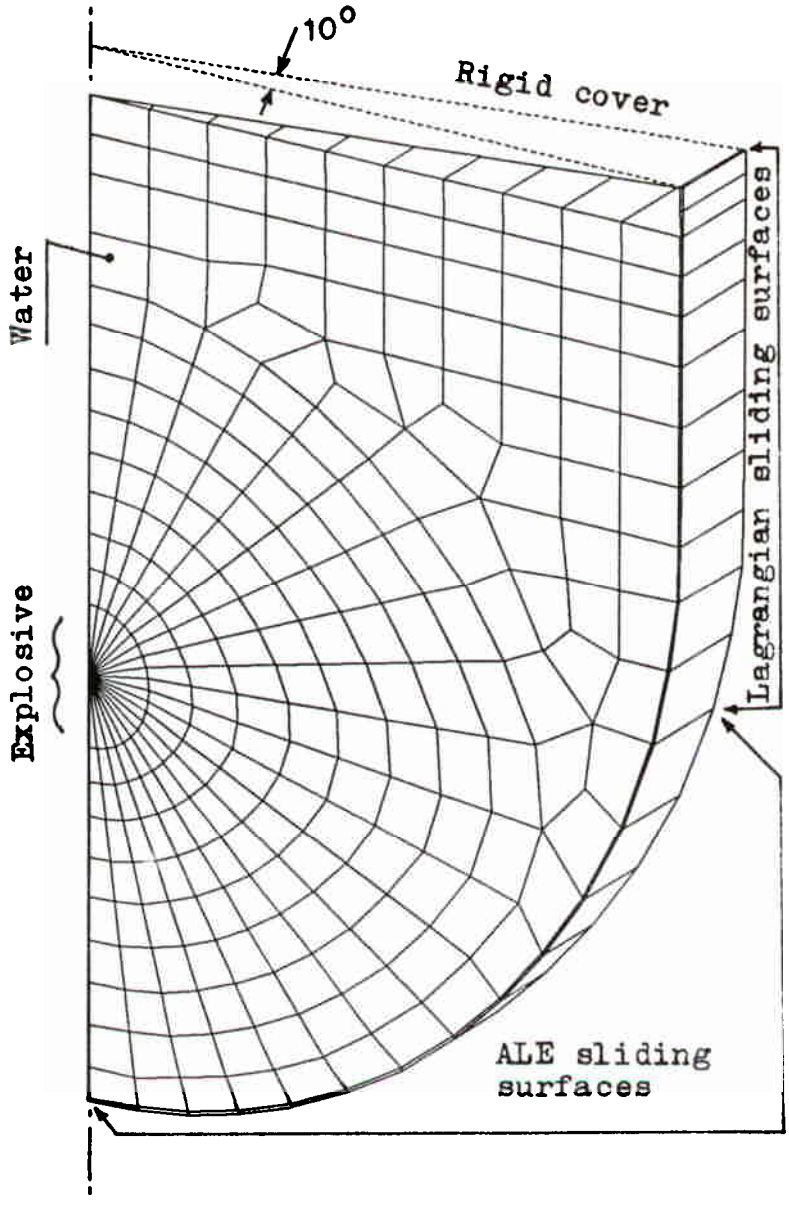

Figure 12: Finite element mesh for thin cylindrical vessel problem

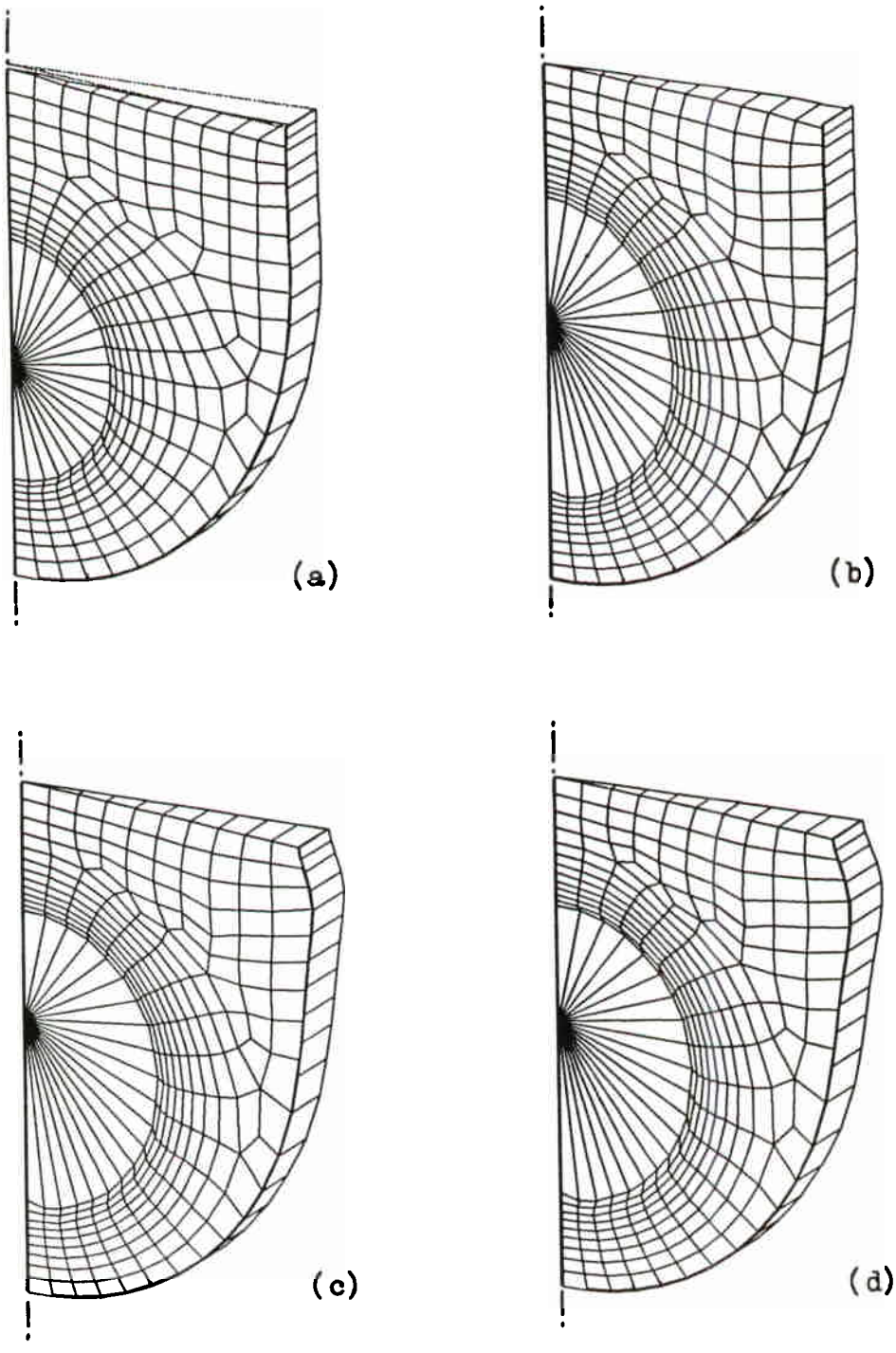

Figure 13: Thin cylindrical vessel problem. Deformed mesh at various times: (a) t=1 ms; (b) t=2 ms; (c) t=3 ms; (d) t=4 ms.

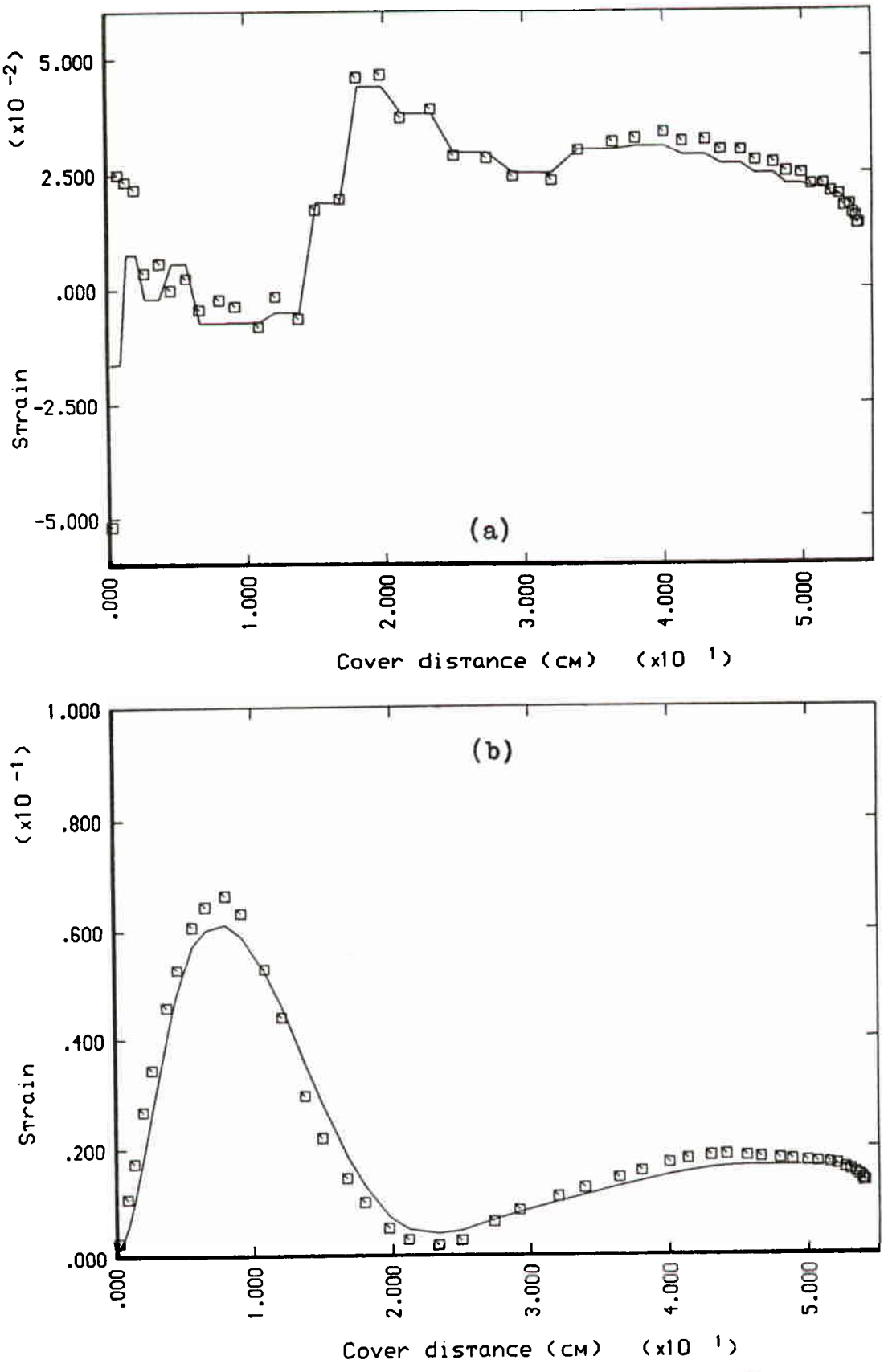

Figure 14: Thin cylindrical vessel problem. Meridional profiles of longitudinal (a) and hoop strain (b): — EURDYN-3M; ⊡ EURDYN-1M (axisymmetric).

References

[1] P. Fasoli-Stella and A.V. Jones, *Survey of computational methods for transient fluid-structure problems in reactor safety,* Advanced Structural Dynamics, J. Donea ed.,Applied Science Publishers, 1980, pp. 191-253.

[2] T. Belytschko and J.M. Kennedy, *Finite element approach to pressure wave attenuation by reactor fuel subassemblies,* J. Press. Technology, 1975, pp. 172-177.

[3] J. Donea, P. Fasoli-Stella and S. Giuliani, *Finite element solution of transient fluid-structure problems in Lagrangian coordinates,* Proc. Internat. Meeting on Fast Reactor Safety and Related Physics, Chicago, 1976, Vol. III, pp. 1427-1435.

[4] W.F. Noh, *CEL : A time-dependent, two-space dimensional, coupled Eulerian-Lagrangian code,* B. Adler et al., eds., Methods in Computational Physics, Academic Press, New York, 1964, p. 117.

[5] J.G. Trulio, *Theory and structure of the AFTON codes,* Air Force Weapons Laboratory, Kirtland Air Force Base Rept. No. AFWL-TR-66-19, 1966.

[6] C.W. Hirt, A.A. Amsden and J.L. Cook, *An arbitrary Lagrangian-Eulerian computing method for all flow speeds,* J. Comput. Phys. 14, 1974, pp. 227-253.

[7] T.J.R. Hughes, W.K. Liu and T.K. Zimmermann, *Lagrangian-Eulerian finite element formulation for inconpressible viscous flows,* US-Japan Seminar on Interdisciplinary Finite Elemet Analysis, Cornell University, Ithaca, NY, 1979.

[8] T. Belytschko and J.M. Kennedy, *Computer models for subassembly simulation,* Nucl. Engrg. Des. 49, 1978, pp. 17-38.

[9] T. Belytschko, J.M. Kennedy and D.F. Schoeberle, *Quasi-Eulerian finite element formulation for fluid-structure interaction,* paper 78-

PVP-60, Joint ASME/CSME Pressure Vessels and Piping Conference, Montreal, Canada, 1978.

[10] J. Donea, P. Fasoli-Stella and S. Giuliani, *Lagrangian and Eulerian finite element techniques for transient fluid-structure interaction problems,* paper B1/2, Trans. 4th Internat. Conf. on Structural Mechanics in Reactor Technology, San Francisco, 1977.

[11] J. Donea, P. Fasoli-Stella, S. Giuliani, J.P.Halleux and A.V. Jones, *An arbitrary Lagrangian-Eulerian finite element procedure for transient dynamic fluid-structure interaction problems,* paper B1/3, Trans. 5th Internat. Conf. on Structural Mechanics in Reactor Technology, Berlin, 1979.

[12] C. Truesdell and R. Toupin, *The classical field theories,* Encyclopedia of Physics, Vol. III 1, Springer, Berlin, 1960.

[13] J. Donea, *Finite element analysis of transient dynamic fluid-structure interaction,* Advanced Structural Dynamics, J. Donea ed., Applied Science Publishers, 1980, pp. 255-290.

[14] J. Donea, P. Fasoli-Stella, S. Giuliani, J.P.Halleux and A.V. Jones, *The computer code EURDYN-1M for transient dynamic fluid-structure interaction,* EUR 6751, Commission of the European Communities, 1980.

[15] J. Donea, S. Giuliani and J.P. Halleux, *An Arbitrary Lagrangian-Eulerian Finite Element Method for Transient Dynamic Fluid-Structure Interactions,* Computer Methods in Applied Mechanics and Engineering, Vol. 33, pp. 689-723, 1982.

[16] S. Giuliani, *An Algorithm for Continuous Rezoning of the Hydrodynamic Grid in Arbitrary Lagrangian-Eulerian Computer Codes,* Nuclear Engineering and Design, Vol. 72, pp. 205-212, 1982.

[17] J. Donea and S. Giuliani, *Fluid -Structure Interaction in Problems with Interfaces Involving Sharp Corners,* 6th International Conference on SMIRT, paper B1/3, Paris, 17-21 August, 1981.

[18] J. Donea, S. Giuliani and J.P. Halleux, *Recent Improvements of the Non-linear Transient Dynamic Structural Computer Programs EUR-DYN,* Commission of the European Communities, EUR 6694, 1980.

[19] I.G. Cameron, N.E. Hoskin and M.J. Lancefield. *Charge Development and Analysis of Recent UK Experiments in the COVA Model Test Programme,* 4th International Conference on SMIRT, paper E2/1, San Francisco, USA, 15-19 August, 1977.

[20] J. Donea, *Arbitrary Lagrangian-Eulerian Finite Element Methods,* Chapter 10 in *Computational Methods for Transient Analysis,* T. Belytschko and T.J.R. Hughes editors, North-Holland, 1983.

[21] T. Belytschko, *Explicit Time Integration of Structure-Mechanical Systems,* Advanced Structural Dynamics, J. Donea ed., Applied Science Publishers, London, 1980.

[22] S.W. Key, *Improvement in Transient Dynamic Time Integration with Application to Spent Nuclear Fuel Shipping Cask Impact Analyses,* Europe-Us Symposium, Volume 2, The University of Trondheim, The Norwegian Institute of Technology, Trondheim, Norway, August 12-16, 1985.

[23] M.L.Wilkins, R.E. Blum, E. Cronshagen and P. Grantham, UCRL-51574 Rev. 1, Lawrence Livermore Laboratory, May 30, 1975.

[24] D.P. Flanagan and T. Belytschko, *A Uniform Strain Hexahedron and Quadrilateral with Orthogonal Hourglass Control,* International Journal for Numerical Methods in Engineering, Vol. 17, pp. 679-706, 1981.

[25] T.J.R. Hughes and W.K. Liu, *Nonlinear Finite Element Analysis of Shells: Part I - Three-dimensional Shells,* Comp. Meth. Appl. Mech. Eng., 26, pp. 331-362, 1981.

[26] T.J.R. Hughes and W.K. Liu, *Nonlinear Finite Element Analysis of Shells: Part II - Two-dimensional Shells,* Comp. Meth. Appl. Mech. Eng., 27, pp. 167-181, 1981.

[27] T.J.R. Hughes, W.K. Liu and I. Levit, *Nonlinear Dynamic Finite Element Analysis of Shells,* In "Nonlinear Finite Element Analysis in Structural Mechanics", W. Wunderlich et al. ed., Springer, Berlin, 1981.

[28] T.J.R. Hughes and E. Carnoy, *Nonlinear Finite Element Shell formulation Accounting for Large Membrane Strains,* Comp. Meth. Appl. Mech. Eng., 39, pp. 69-82, 1983.

[29] F. Casadei, *A Nonlinear 3-D Shell Element Implementation for Transient Problems,* Commission of the European Communities, EUR report (in preparation).